Journal of Vacuum Science and Technology A

RESEARCH ARTICLE | MAY 29 2025

Rules of triplet state electron impact neutral dissociation in plasma from molecular dynamics simulations and an electrophore model

Ryan Brook ; Oliver Bramley ; Dmitry V. Makhov ; Anna Nelson ; Gregory Armstrong ; Joseph Yong ; Ezri Saunders ; Johnny de Viggiani ; Jonathan Tennyson ; Dmitrii V. Shalashilin

Check for updates

J. Vac. Sci. Technol. A 43, 043003 (2025)
https://doi.org/10.1116/6.0004454

View Online
Export Citation

29 May 2025 13:06:07

JVST A
Journal of Vacuum Science & Technology A

ARTICLE

pubs.aip.org/avs/jva

Rules of triplet state electron impact neutral dissociation in plasma from molecular dynamics simulations and an electrophore model

Cite as: J. Vac. Sci. Technol. A 43, 043003 (2025); doi: 10.1116/6.0004454
Submitted: 3 February 2025 · Accepted: 16 April 2025 ·
Published Online: 29 May 2025

View Online Export Citation CrossMark

Ryan Brook,[1,a)] Oliver Bramley,[2] Dmitry V. Makhov,[1] Anna Nelson,[2] Gregory Armstrong,[2] Joseph Yong,[1] Ezri Saunders,[1] Johnny de Viggiani,[1] Jonathan Tennyson,[2,3] and Dmitrii V. Shalashilin[1,b)]

AFFILIATIONS

[1]School of Chemistry, University of Leeds, Leeds LS2 9JT, United Kingdom
[2]Quantemol Ltd., 320 City Road, The Angel, London EC1V 2NZ, United Kingdom
[3]Department of Physics and Astronomy, University College London, London WC1E 6BT, United Kingdom

[a)]**Electronic mail:** cm18rb@leeds.ac.uk
[b)]**Electronic mail:** d.shalashilin@leeds.ac.uk

ABSTRACT

Electron impact driven neutral dissociation of molecules that is important in low temperature plasma is investigated. Despite its importance for plasma technologies in microelectronics manufacturing, this process has received almost no attention from the computational chemistry community, which for decades has been focused on photodissociation. Simulations are performed for the dissociation of several fluorinate-organic molecules in their lowest triplet state, populated via electron impact excitation. Their dissociation in plasmas has recently been studied experimentally and their dissociation pathways have been shown to differ from those of the singlet ground state. Rules that determine the dissociation pathways in fluorinate-organic molecules are proposed and rationalized via analysis of an ensemble of trajectories, highlighting the common dissociation pathways. These rules can help to find new molecules for use in future plasma technologies, which produce a desired chemical composition of plasma, enhancing selectivity, etch rates, and environmental benefits.

© 2025 Author(s). All article content, except where otherwise noted, is licensed under a Creative Commons Attribution (CC BY) license (https://creativecommons.org/licenses/by/4.0/). https://doi.org/10.1116/6.0004454

29 May 2025 13:06:07

I. INTRODUCTION

In this work, we will use our experience in photochemistry and molecular dynamics to apply the methodology developed there in the novel context of dissociation following electron impact. In photochemistry,[1] the photon wavelength usually lies within the visible to the ultra-violet region,[2] while in typical low temperature plasma, used in manufacturing, the temperature of the molecules is about $\sim 10^3$ K. However, excitation occurs via impact of an electron that has the energy of several eV, see Ref. 3. In both photoexcitation and electron impact excitation, a molecule M is raised to a higher electronic state M^*; see Fig. 1. Subsequently, it evolves on the potential energy surface (PES) of this excited state from which it is possible for the molecule to transfer to another electronic state via a quantum nonadiabatic process known as internal conversion. It is quite common for relaxation from an excited state to occur via dissociation and, as a result, the molecule M can dissociate into neutral free radicals A• and B•,

$$M + e^- \rightarrow A\bullet + B\bullet + e^-. \quad (1)$$

Figure 1 illustrates the dissociative motion of a quantum wave packet representing nuclear motion in molecule M^*.

Photoabsorption selection rules dictate that for a closed shell target molecule, excited molecule M^* occurs as a singlet electronic state, whereas excitation via electron impact can give both singlet and triplet states. At low electron collision energies, excitation of the triplet state that is generally lower lying is usually favored. However,

© Author(s) 2025

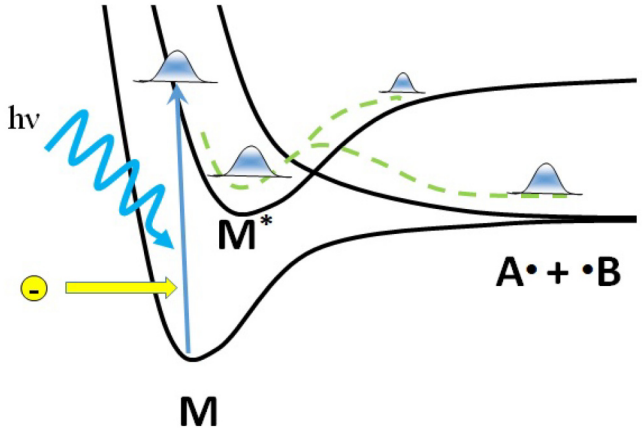

FIG. 1. Similarity between dynamics after photon absorption and electron impact. A key difference is that the photoexcited molecule M^* is always in a singlet state, but in the case of electron impact M^*, it often represents a triplet state of the molecule.

the methodology developed to simulate singlet states dynamics in photochemistry can be directly transferred for use in triplet state dynamics.[4] So far, the dynamics of triplet states have been largely overlooked, as attention has been focused almost entirely on photochemistry and singlet excited states.[5–10] Triplet states in photochemistry are generated from singlet states via intersystem crossing and, therefore, occur only on longer time scales[2] and their dynamics are very different from that after electron impact.

Neutral dissociation of fluorinated organic molecules in plasmas is of significant interest as such molecules are employed in multiple plasma technologies.[11–14] The radicals produced via the dissociation of these molecules play a pivotal role in plasma etching or plasma deposition.[15–18] When designing new plasma technologies involving novel feedstock gases, it is important to know the channels of dissociation to ensure desirable properties of technological processes, such as an increase in selectivity or the etch rate. Furthermore, molecules chosen for this process are often perfluoroalkyl substances such as PFAS chemicals.[19,20] Due to their high global warming potential (GWP), these have been dubbed "Forever Chemicals" and are environmentally concerning;[21–23] as a result, there has been great effort employed in the search for alternatives.[15,24–30] By understanding the mechanism for dissociation and how this is controlled by molecular composition and structure, it should be possible to design technologically useful molecules, which are highly efficient and predictable and which have lower environmental impact. Thus, there is great interest in investigating chemistry after electron impact in plasma theoretically,[15,31–35] with the area of neutral dissociation being labeled as "one of the least studied yet most important."[16]

II. THEORY

A. Electrophore model

Previously, our group presented a work detailing the simulations of the dissociation dynamics of two small hydrofluorocarbon molecules, $C_3H_2F_6$ and $C_3H_2F_4$,[4] which underwent neutral dissociation from an excited triplet state. Triplet states have been shown to be important in the dissociation of plasma through molecular orbital calculations.[36] The initial triplet states were chosen on the basis of electron impact excitation cross sections generated by Quantemol's Electron Collision (QEC)[37] expert system, which uses the UKRmol+R-matrix codes;[38] it was also shown that only the lowest lying triplet state needed to be considered. As a result of this behavior, dynamics need to be performed on the lowest lying triplet state only, thereby significantly reducing the computational cost. The presence of a C═C bond in the molecule was found to play a pivotal role in determining the dissociation of molecules after the electron impact.[4] Our calculations suggested that electron impact excites a small area of the molecule, such as the carbon–carbon double bond (C═C). If a double carbon–carbon (C═C) bond was present, the lowest triplet state was the only state that was populated, or in the absence of a C═C bond, all higher excited triplet states rapidly relaxed down to the lowest lying triplet state. This group can be called an electrophore, by analogy with the chromophore group in photochemistry. The excited electrophore affects the neighboring chemical bonds, which break first, influencing the neutral dissociation pathways and chemical composition of plasma as the distance from a C═C bond was found to determine how often a C—F bond broke. The importance of the double C═C bond and the fact that it becomes much weaker in plasma has been known for some time[39] but had not been fully investigated through dynamics calculations. In this paper, we investigate more molecules and develop the ideas of Ref. 4 further.

In Sec. III, we show that our calculations can be interpreted by the following novel "electrophore" model, illustrated by Fig. 2. Figure 2(a) sketches the molecular orbital diagram of a C═C bond. The C═C double bond plays the role of an electrophore due to a low energy gap between the bonding orbitals forming a C═C double bond. After the electron impact, an electron is annihilated from the bonding π orbital and an electron is created in the antibonding π^* orbital of the double bond forming the lowest triplet state, which weakens the double bond. The electron density can then be donated to the antibonding orbitals of the neighboring bonds, weakening them and causing the observed higher number of dissociation events in the vicinity of the double bond electrophore.

Due to its lone pairs, the oxygen atom —O— can also play the role of an electrophore, localizing the triplet excitation. Figure 2(b) shows a molecular orbitals diagram, which qualitatively explains the role of lone pairs in the localization of triplet excitation. In the ⋯—C—O—C—⋯ group, the bonds can be described in terms of bonding and antibonding orbitals formed from sp^3 hybridized orbitals of oxygen and carbon atoms as illustrated in the figure. However, four electrons on the lone pairs of oxygen do not participate in bonding and occupy the so-called non-bonding orbitals. As a result, their energy is between that of the bonding and antibonding molecular orbitals making a gap between the lone pair orbital and the lowest antibonding orbital smaller than the gap between the bonding and antibonding orbitals. Electron impact can then easily remove an electron (shown by gray arrows) from the lone pair orbital while causing an electron to occupy the lowest antibonding orbital creating a localized triplet state. It is important that similarly to the case of the double bond shown in Fig. 2(a),

29 May 2025 13:06:07

© Author(s) 2025

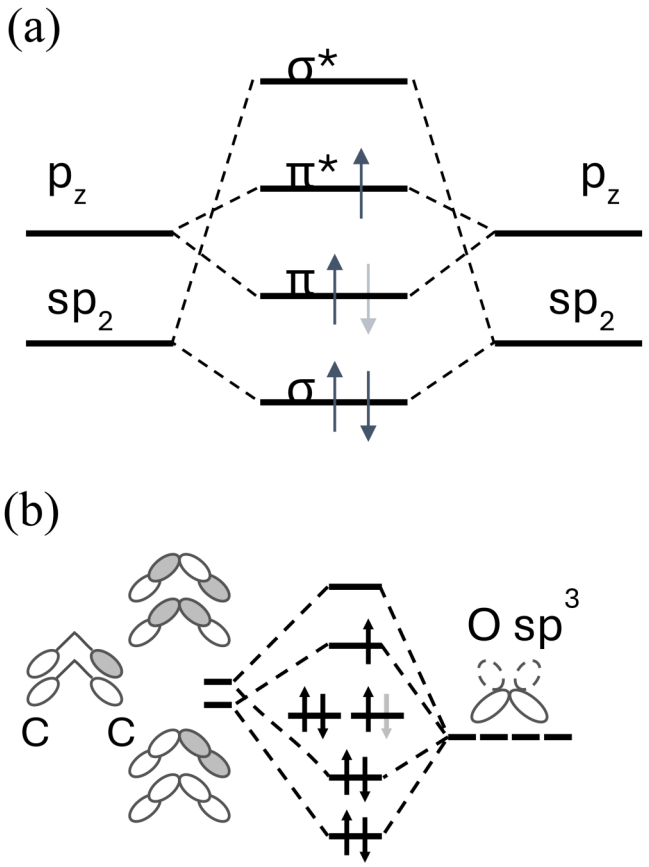

FIG. 2. Molecular orbital diagram of a (a) C═C double bond (a) and (b) C—O—C group electrophores illustrates how triplet excitation can be localized in the region with a low energy gap between the highest occupied and the lowest unoccupied orbitals. (a) shows a low energy gap between the π-orbital and the π*-orbital. The low gap between them ensures localization of excitation in the C═C electrophore when electron impact annihilates an electron from the π-orbital (shown in gray) and generates it on the π*-orbital. (b) shows that lone pairs of the oxygen atom (shown by dashed lines) do not participate in chemical bonding and their energy is in the middle between those of the bonding and antibonding orbitals. Electron impact removes an electron from the lone pair (shown in gray) and puts an electron on the lowest antibonding orbital. The energy gap of this process is lower than that of promoting an electron from the bonding to the antibonding orbital. Electron impact creates a localized triplet state at an electrophore. Then, the triplet state electron density can be donated to the antibonding orbitals of other bonds, close to the electrophore.

there are two pairs of bonding and antibonding orbitals, which make the energy of the lowest antibonding orbital smaller. As electrons are indistinguishable, it is not possible to say whether the electron occupying the antibonding orbital is the displaced electron from the bonding orbital or the impacting electron.

B. Molecules considered

In this work, we investigate a new selection of fluorinated organic molecules that contain an oxygen atom. First, we consider a pair of positional isomers of ether $C_4F_7H_3O$, one containing the methoxy group at the end of the carbon chain[40–44] (n-$C_4F_7H_3O$) and the other with the methoxy group in the middle of the carbon chain[43–46] (i-$C_4F_7H_3O$). We also study a functional group isomer of $C_4F_7H_3O$ where an alcohol group is present[44,47] ($C_4F_7H_2OH$). This allows us to test our supposition that the dissociation pathway is sensitive to both position and functional group isomers of the same general molecular formula. The last molecule presented in the paper, $C_5F_{10}O$[41,43] or perfluoropropyl vinyl ether (PPVE), contains both a carbon—oxygen—carbon (C—O—C) bond and a C═C bond, allowing us to investigate how the presence of both functional groups affects the molecule's dissociation pathways. All of these molecules were chosen due to the recent efforts to determine whether they would make suitable replacements for the standard industry choices for feedstock gases in technological plasmas.[43,44,48]

C. Computational details

For all molecules considered in this paper, the lowest triplet state has a large electron impact excitation cross section at energies up to 15 eV. The excited state cross section calculations for all molecules were done with the QEC software employing a cc-pVDZ basis and using an active space of six electrons in six active orbitals with a vertical cutoff of 15 eV, with the exception of PPVE for which the cutoff was extended to 20 eV. Therefore, all dynamics in this paper are performed on the lowest-lying triplet state, using the standard *ab initio* molecular dynamics. It should be noted that if more than one electronic state is important, *ab initio* multiple cloning[4,49–52] or another method of electronically nonadiabatic dynamics[5,51] can be used in a future calculation, which considers more complex dynamics involving several electronic states. The choice of when to reintroduce nonadiabatic dynamics will require a further investigation into the excited states of larger molecules. In our previous work,[4] spin-flip time-dependent density functional theory (TDDFT)[53] was used to calculate PESs and forces since several excited triplet states were involved. However, after the simplification to a single lowest-lying triplet state, it is reasonable to question the necessity of including spin-flips. Calculations of higher triplet state PESs and associated nonadiabatic coupling matrix elements are not necessary and, therefore, for direct molecular dynamics on the lowest triplet state, a simpler DFT methodology can be used. In the supplementary material, through Figs. S1 and S4, we compare the use of spin-flip TDDFT to standard DFT for each molecule, a choice that saves significant computational cost while providing similar (or even better) accuracy. All energy and force calculations in this paper were performed using the electronic structure package Q-CHEM[54] with a 6-31 + G* basis set and the BHHLYP hybrid functional. We assumed that the triplet state was formed in the collision with the incoming impacting electron very quickly on the time scale of vibrational motion. Therefore, according to the Franck–Condon principle, the initial geometries for the trajectories can be taken as a result of geometric optimization of the molecule in its singlet ground state. The initial momenta are generated from a classic Boltzmann distribution of the relevant temperature for all vibrational modes. The coordinates of each trajectory can then be scanned to find the time of each bond dissociation, allowing for the presentation of dissociation kinetics for an ensemble of trajectories, showing which bonds break most

29 May 2025 13:06:07

© Author(s) 2025

often and most quickly. Each bond environment is averaged by the number of bonds present in the said environment, allowing for the identification of the most efficient dissociative bonds. Additional information can be gleaned from the sequence of broken bonds, providing insight into the most common dissociation pathways.

Initial calculations were performed at $T = 5000$ K. While 5000 K is higher than the temperature of the plasmas studied experimentally or industrially using these molecules,[42,43] it is advantageous to run initial simulations at this temperature to facilitate bond breaking and allow the collection of a large amount of data within a small timeframe (500 fs). We found that an ensemble of 400 trajectories provides statistics sufficient for convergence and conclusions can be drawn about the different dissociation pathways undertaken by the molecule; see Fig. S5 in the supplementary material. To establish the temperature dependence of the dissociation process, trajectories were also run at lower temperatures, namely, 4000 and 3000 K.

III. RESULTS AND DISCUSSION

A. Dissociation pathways in n-$C_4F_7H_3O$ and i-$C_4F_7H_3O$ isomers

1. Overall behavior

First, we compare the n- and i-isomers of $C_4F_7H_3O$ ether, which can be characterized by the placement of oxygen within the molecule. In accordance with the theory proposed in Sec. II A that the oxygen atom plays a pivotal role in triplet state dissociation, we expect to observe a slightly different dissociative behavior. Figures 3 and 4 show the electron impact excitation cross sections of the lowest electronic states, and as predicted, the lowest excited state in both molecules is a triplet state. As shown in Fig. 3, the n-$C_4H_3F_7O$ molecule exhibits a

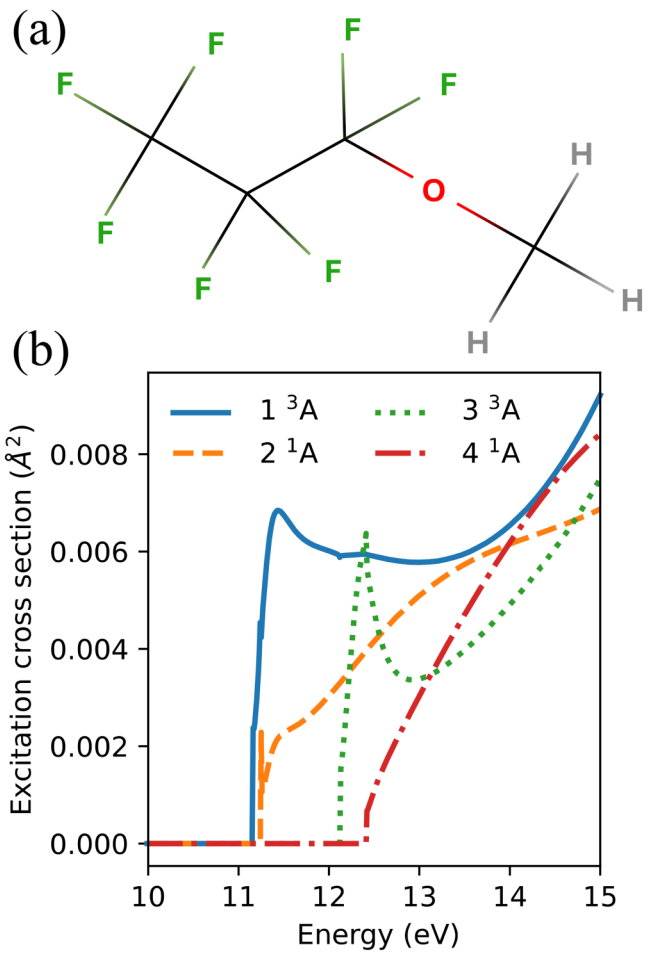

FIG. 3. (a) Molecular structure of n-$C_4H_3F_7O$ with its (b) electron impact excitation cross sections calculated using QEC.

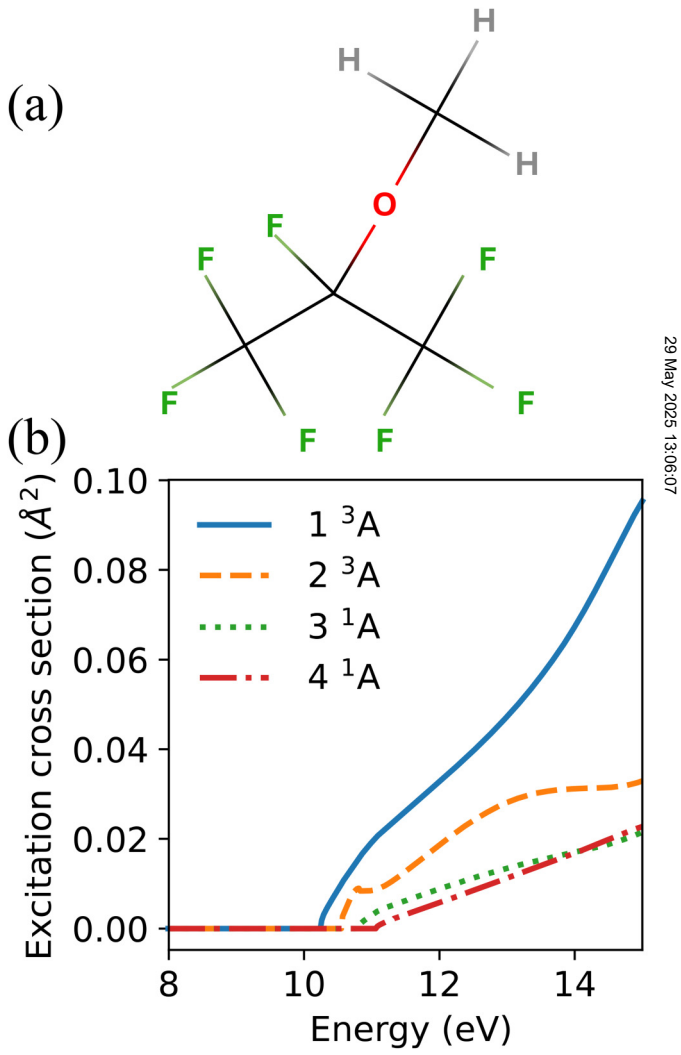

FIG. 4. (a) Molecular structure of i-$C_4H_3F_7O$ with its (b) electron impact excitation cross sections calculated using QEC.

29 May 2025 13:06:07

© Author(s) 2025

significant energy gap between the lowest excited state (triplet) and the next excited state, which is a singlet. For the case i-$C_4H_3F_7O$, shown in Fig. 4, the two lowest energy cross sections are those of the triplet states, the lowest of which has the largest cross section across the whole energy range considered. Thus, for both positional isomers, the lowest is the triplet state with a much larger excitation cross section than the singlet state, meaning it is reasonable to assume that the neutral dissociation dynamics occur upon the lowest triplet state.

Figure 5 shows the overall dissociation kinetics for n-$C_4H_3F_7O$. This isomer contains both two C—C and two C—O bonds and despite the C—O bonds initially breaking much earlier in the propagation, by 500 fs, the two bond types dissociate roughly an equal number of times, with 35% of the C—C bonds dissociating and 36% of the C—O bonds dissociating. The C—H bonds also dissociate readily with 27% of the C—H bonds breaking, with a significant percentage of dissociation events occurring within 25 fs. Despite being the most abundant bond type, the C—F bonds break on average the least with only 4.1% of C—F bonds dissociating.

The other positional isomer is i-$C_4H_3F_7O$, where the methoxy group in the middle of the carbon chain, is now considered, with the dissociation kinetics for the different bond types shown in Fig. 6. This isomer has greater symmetry, with two CF_3 groups on either

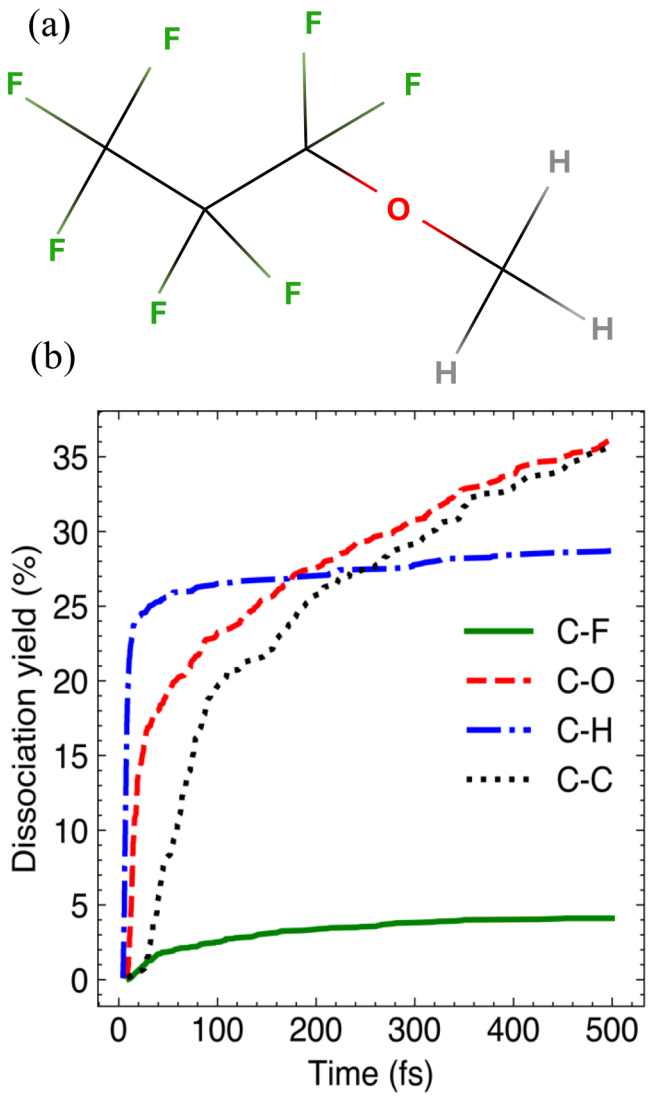

FIG. 5. (a) Molecular structure of n-$C_4F_7H_3O$ and (b) the comparison of the dissociation kinetics for its different bonds at 5000 K.

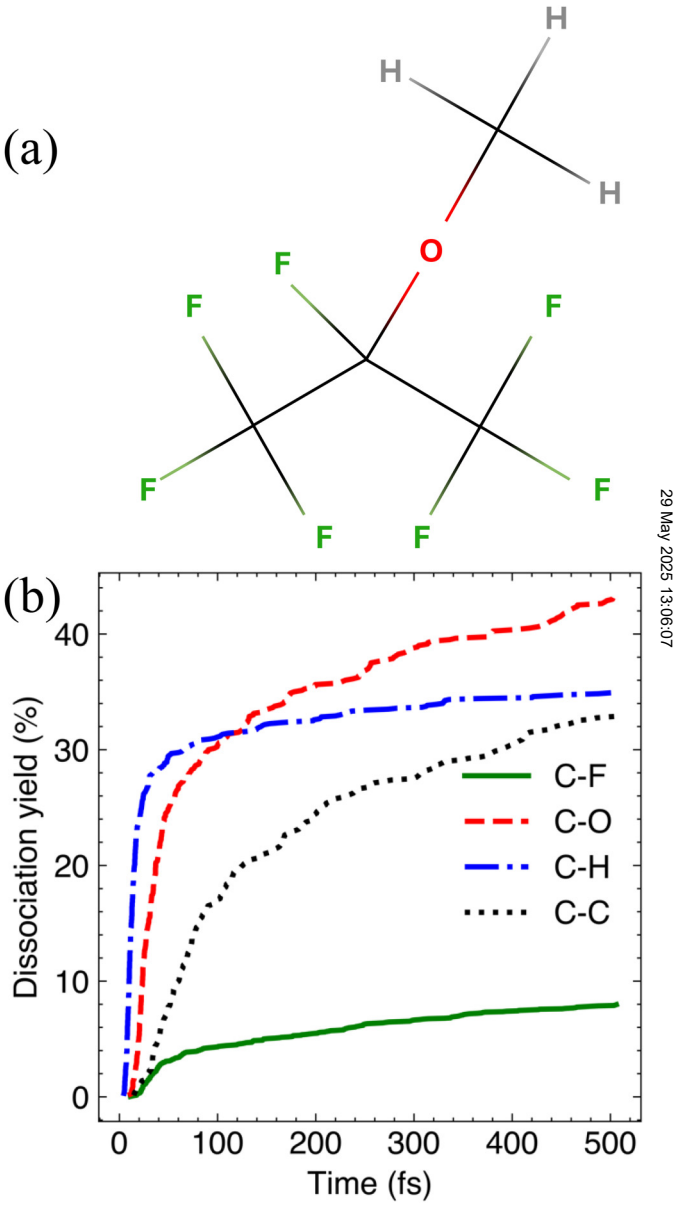

FIG. 6. (a) Molecular structure of i-$C_4F_7H_3O$ and (b) the comparison of the dissociation kinetics for its different bonds at 5000 K.

29 May 2025 13:06:07

© Author(s) 2025

side of the methoxy group. As expected, positional isomers have similar dissociation patterns. However, while the order of bond type breaking is maintained the same in both isomers, all bond types other than the C—C bonds break more frequently in the symmetrical i-isomer. 35% of the C—H bonds dissociate, and as multiple hydrogens leaving the same carbon is discouraged, most trajectories have a C—H bond breaking. The dissociation yield of the C—O bonds also increases to approximately 43%. Compared to the n-isomer, the number of C—F bonds dissociating in the i-isomer is roughly two times greater at 8% of the C—F bonds broken. The overall increase in dissociation events suggests that the symmetrical structure of the i-$C_4H_3F_7O$ isomer is more conducive to bond dissociation, including the least broken C—F bonds.

2. C–O bonds

As seen in Figs. 5 and 6, there are a larger number of C—O bonds dissociating in i-$C_4F_7H_3O$ than in *n*-$C_4F_7H_3O$. Figures 7 and 8 compare the dissociation of individual C—O bonds present in both isomers, revealing different behaviors. For n-$C_4H_3F_7O$, the C#4—O bond has many dissociation events within the first 100 fs, whereas the number of C#3—O bonds broken increases in a more linear fashion. By 500 fs, the number of dissociations of each C—O bond environment becomes roughly equal with C#3—O contributing 52.5% and C#4—O 47.5% of the total number of C—O bond dissociations. For i-$C_4H_3F_7O$, there is a greater difference in dissociation yields between the two bonds, with C#2—O accounting for 63.7% of the total number of C—O bonds dissociated, and C#4—O contributing 36.3%. In both isomers, breaking of the C#4—O bond results in the dissociation of a methyl group from the oxygen atom. Despite this process starting faster in the n-isomer, the final average number of dissociation events is similar in both isomers. The C#4—O bond has a dissociation yield of 33% in n-$C_4H_3F_7O$ and 31% in i-$C_4H_3F_7O$. Thus, the difference in the C—O bond breaking events between the isomers is due to the C#2—O bond in i-C_4H_3F dissociating more often than the C#3—O bond in n-$C_4H_3F_7O$, with 55% and 37% dissociation yields, respectively. This difference can be explained by the stability of the radicals formed after bond dissociation. Severance of the C#3—O bond in n-$C_4H_3F_7O$ results in a radical on the terminal carbon, which is less favorable than the radical in the middle of the carbon chain formed by the dissociation of the C#2—O bond in i-$C_4H_3F_7O$. The symmetrical radical experiences the stabilizing effects of carbon on either side of the radical, due to increased hyperconjugation and inductive effects from the increased number of adjacent atoms.

3. C–C bonds

Figures 9 and 10 compare the breaking of individual C—C bonds in both n-$C_4F_7H_3O$ and i-$C_4F_7H_3O$. As expected in a more symmetrical molecule, i-$C_4H_3F_7O$, both C—C bonds dissociate at approximately similar rates, with a small difference in the final percentages of the total C—C dissociations of 53% to 47%. The picture is more interesting in the n-$C_4H_3F_7O$ isomer, where the C#2—C#3 bond breaks more often than the C#1—C#2 bond with a ratio of 64%–36% of the total C—C dissociations in n-$C_4H_3F_7O$. This ratio can be explained through the effect of the oxygen atom. As discussed in Sec. II A, the oxygen atom

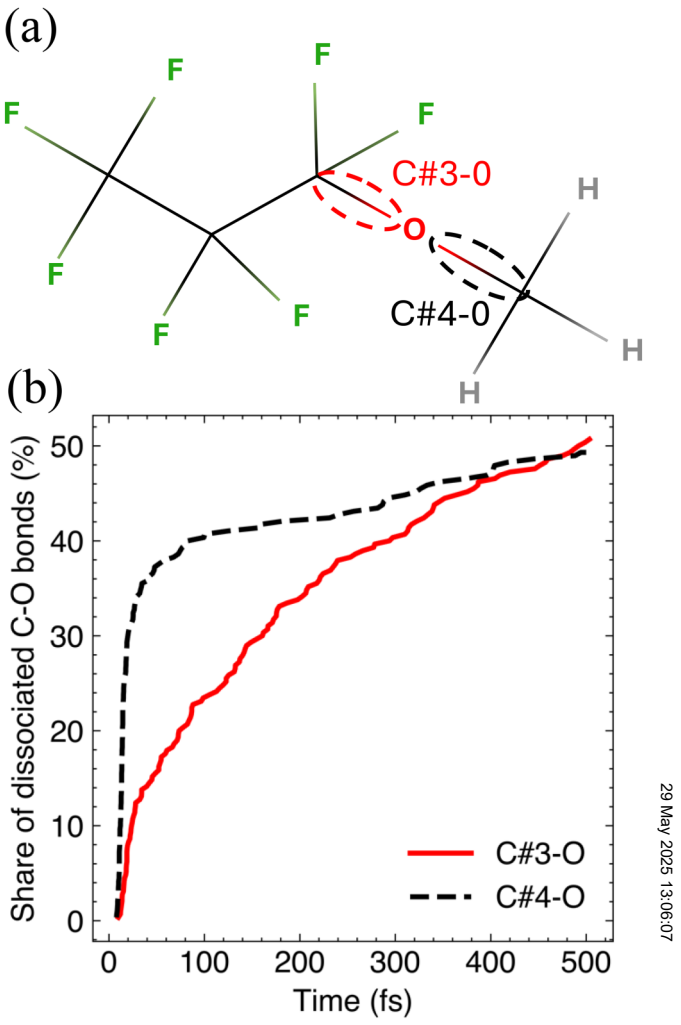

FIG. 7. (a) Molecular structure of n-$C_4F_7H_3O$ highlighting the different C—O environments, C#3—O (red solid line), and C#4—O (black dashed line) and (b) the comparison of the dissociation kinetics for the C—O bonds in n-$C_4F_7H_3O$ at 5000 K. The average number of dissociations per bond in each environment is shown as a percentage of the total number of C—O bond dissociations for 500 fs.

electrophore being on a terminal chain position means that the triplet state localization effect more heavily affects the closest C—C bond resulting in the difference seen.

4. C–F bonds

Similarly, the position of the oxygen atom in n-$C_4F_7H_3O$ determines the ratio by which different C—F environments dissociate, shown in Fig. 11. In n-$C_4F_7H_3O$, two C—F bonds on the same carbon as oxygen (C#3—F) accounts in total for 52% of all C—F bonds broken (26% each) despite making up only 29% of the C—F bonds in the molecule. Moreover, even though there are three

29 May 2025 13:06:07

© Author(s) 2025

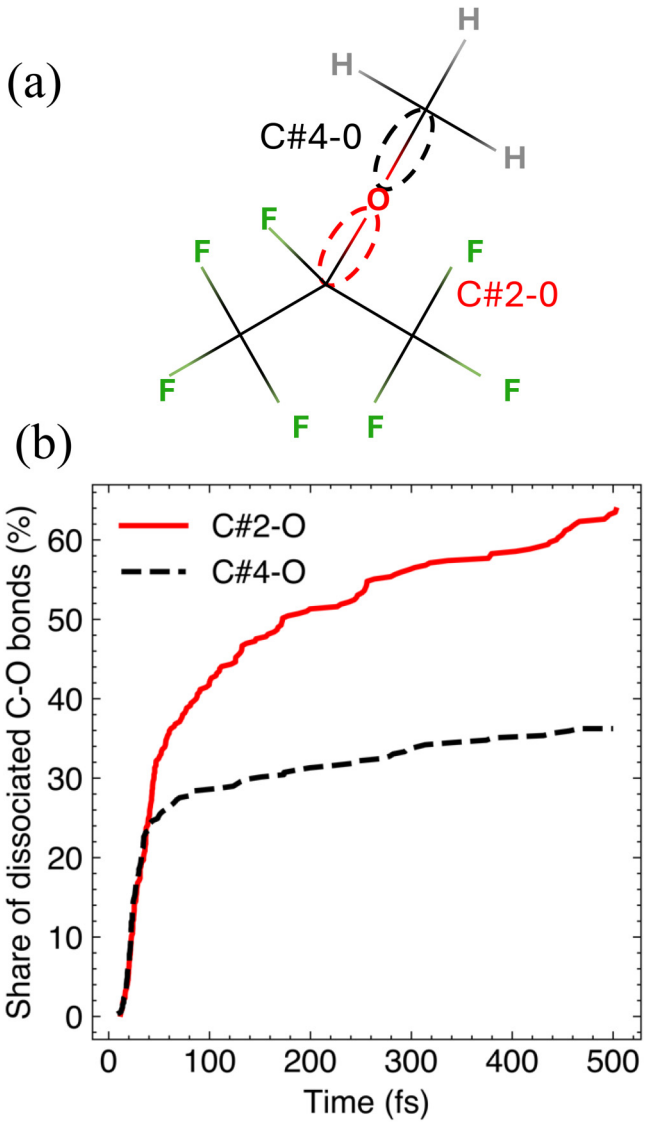

FIG. 8. (a) Molecular structure of i-$C_4F_7H_3O$ highlighting the different C—O environments, C#2—O (red solid lines), and C#4—O (black dashed line) and (b) the comparison of the dissociation kinetics for different C—O bonds in i-$C_4F_7H_3O$ at 5000 K. The average number of dissociations per bond in each environment is shown as a percentage of the total number of C—O bond dissociations for 500 fs.

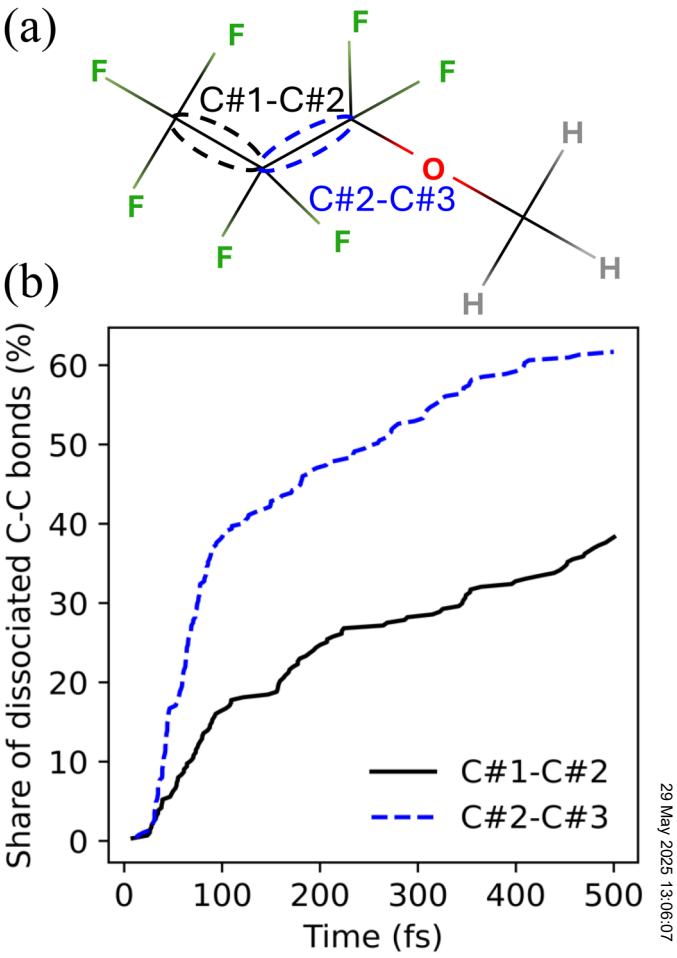

FIG. 9. (a) Molecular structure of n-$C_4F_7H_3O$ highlighting the different C—C environments, C#1—C#2 (black solid line), and C#2-C#3 (blue dashed line) and (b) the comparison of the dissociation kinetics for different C—C bonds in n-$C_4F_7H_3O$ at 5000 K. The average number of dissociations per bond in each environment is shown as a percentage of the total number of C—C bond dissociations for 500 fs.

C#1—F bonds compared to the two C#2—F bonds, they dissociate with a similar frequency. By 500 fs, the percentage of dissociated C—F bonds attributed to C#1—F and C#2—F are 23.9% and 24.7%, respectively. A second dissociation event involving a particular atom is generally discouraged. Hence, it might be expected that because C#2—C#3 is the most broken C—C bond, this would make the breaking of C#3—F less favorable. The fact that this is not observed reinforces the strength of the impact that the electrophore oxygen atom has that on the dissociation of other bonds. The closer the C—F bond is to the electrophore, the more readily it dissociates.

Similarly, for i-$C_4F_7H_3O$, the order of the efficiency of C—F environments can be determined by their proximity to the electrophore oxygen atom, as shown in Fig. 12. The C#1—F and C#3—F environments account for 40% and 32.7% of the C—F bonds dissociated in i-$C_4F_7H_3O$, respectively. In our simulations, the methyl group bonded to the oxygen atom is not, in fact, planar with the oxygen atom and is directed more toward C#1 than C#2. In experiments, this bond would be constantly rotating, producing two equally likely conformers, where the methyl group is directed toward either C#1 or C#3, meaning that these two isomers are indistinguishable in reality and, therefore, the molecule can be

29 May 2025 13:06:07

© Author(s) 2025

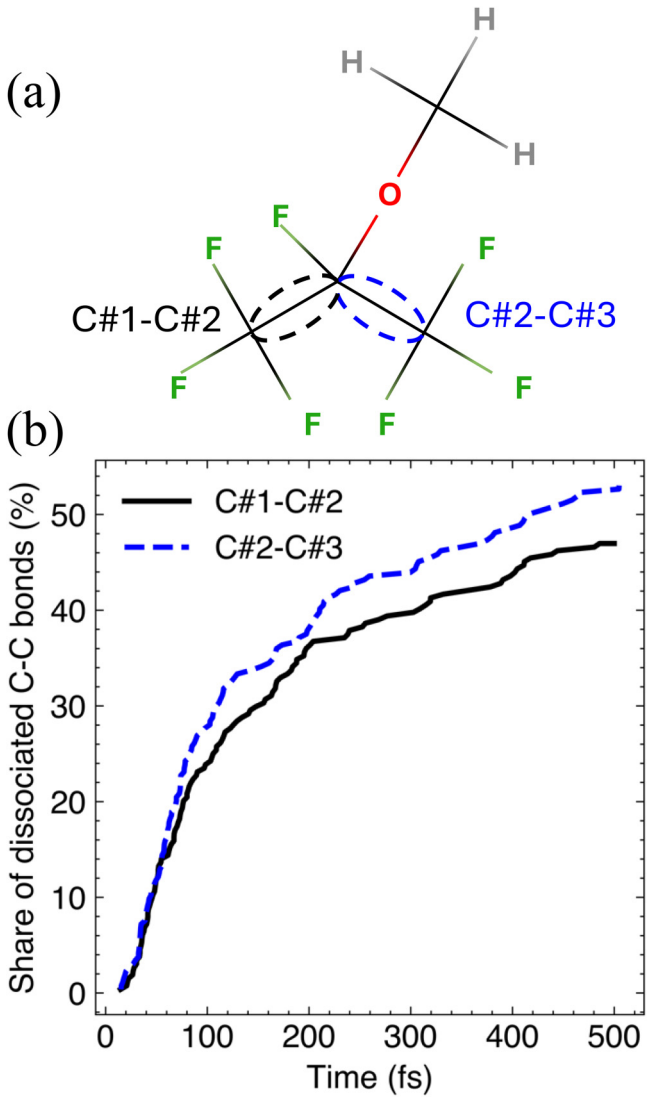

FIG. 10. (a) Molecular structure of i-$C_4F_7H_3O$ highlighting the different C—C environments, C#1—C#2 (black solid line), and C#2—C#3 (blue dashed line) and (b) the comparison of the dissociation kinetics for different C—C bonds in i-$C_4F_7H_3O$ at 5000 K. The average number of dissociations per bond in each environment is shown as a percentage of the total number of C—C bond dissociations for 500 fs.

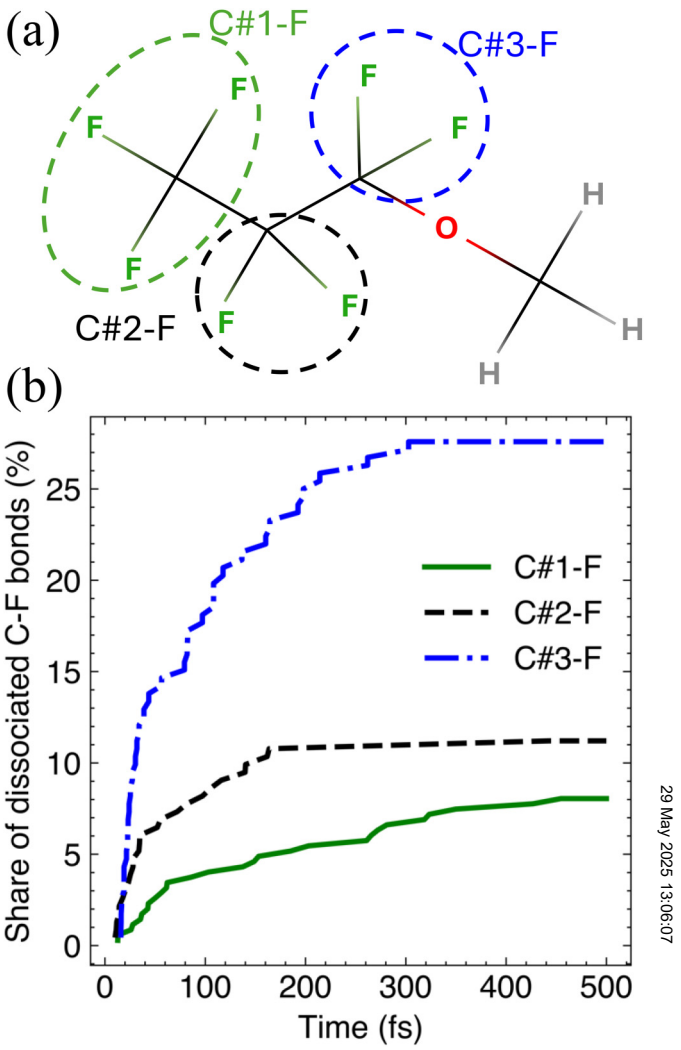

FIG. 11. (a) Molecular structure of n-$C_4F_7H_3O$ highlighting the different C—F environments, C#1—F (green solid line), C#2—F (black dashed line), and C#3—F (blue dashed–dotted line) and (b) the comparison of the dissociation kinetics for different C—F bonds in n-$C_4F_7H_3O$ at 5000 K. The average number of dissociations per bond in each environment is shown as a percentage of the total number of C—F bond dissociations for 500 fs.

considered, in practice, to be symmetrical. However, due to each trajectory for i-$C_4F_7H_3O$ beginning from a single optimized geometry, only one of these conformers is considered in our simulations, and in calculations, we can distinguish between C#1 or C#3. In the optimized geometry used in this paper, the fluorine atoms attached to C#1 carbon have an average distance to the hydrogen atoms of 6.13, 6.81, and 10.07 bohr, respectively, compared to the average distance to the hydrogens of the fluorine atoms bonded to C#3 of 9.79, 9.47, and 10.80 bohr. The C#1—F bonds can, therefore, be seen as more sterically favored to dissociate when compared to the C#3—F bonds as the dissociation will release some of the strain experienced by the molecule. This trend is further supported by the fact that the fluorine bonded to C#1 that has the shortest distance to a hydrogen atom is the C—F bond that dissociates the most out of the C#1—F and the C#3—F C—F bonds. Due to a small total number of C—F bonds being broken, the difference between C#1—F and C#3—F is small when averaged by the number of bonds present within the environment, with dissociation yields of 7.5% and 6.0%, respectively, and each C#1—F bond accounts for 13.4% of the C—F dissociations compared to 10.9% of the C—F

29 May 2025 13:06:07

© Author(s) 2025

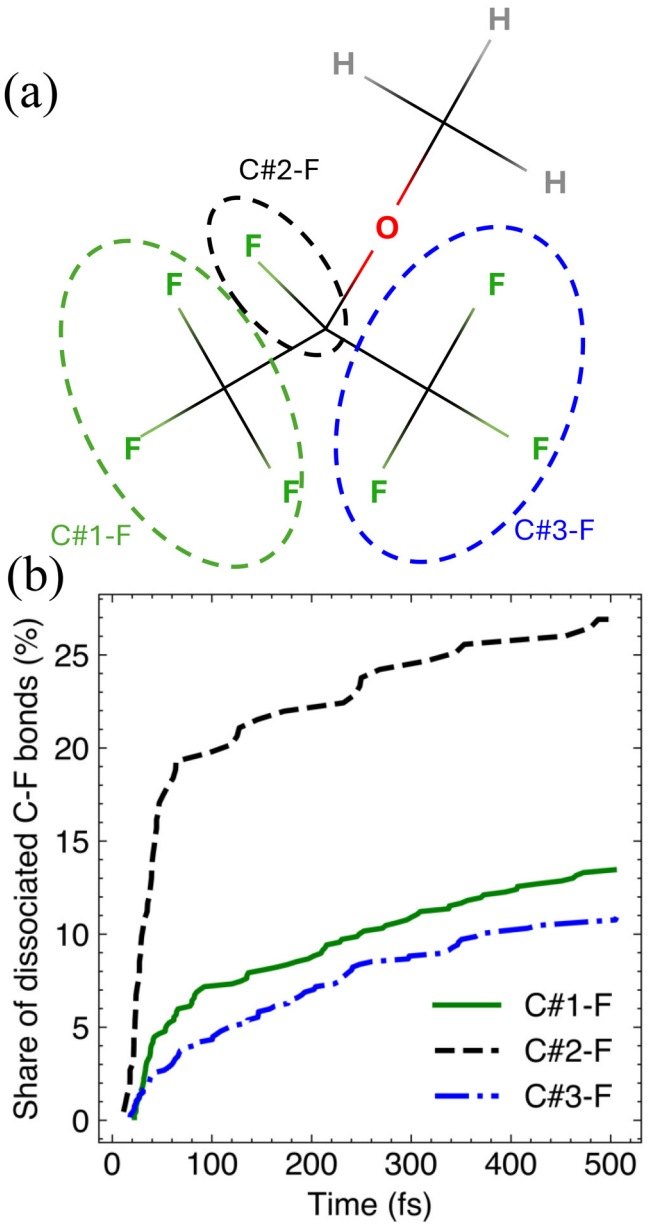

FIG. 12. (a) Molecular structure of i-$C_4F_7H_3O$ highlighting the different C—F environments, C#1—F (green solid line), C#2—F (black dashed line), and C#3—F (blue dashed–dotted line) and (b) the comparison of the dissociation kinetics for different C—F bonds in i-$C_4F_7H_3O$ at 5000 K. The average number of dissociations per bond in each environment is shown as a percentage of the total number of C—F bond dissociations for 500 fs.

dissociations being each of the C#3—F bond. The single C#2—F bond represents 26.9% of all C—F dissociation events, with a dissociative yield of 15%. This is due to being bonded to the same carbon as the electrophore, causing a more severe weakening of the bond than the other C—F environments that are bonded to the adjacent carbons. As the dissociation of a bond discourages another bond involving those atoms from breaking, the dissociation of the C#2—F bond is discouraged by either the C—C bond or the C#2—O bond dissociating. Similarly, the dissociation of a C#1—F or C#3—F bond is discouraged by only one of the C—C bonds or the equivalent C—F environment. Therefore, the conditions that limit the dissociation of C#1—F and C#3—F occur significantly less often than the factors impacting the dissociation of C#2—F. Despite this, the C#2—F bond has a higher dissociative yield, suggesting that the dissociation happens very readily, due to the proximity to the oxygen atom.

5. Temperature dependence

The temperature dependence of the fragmentation pathways for both molecules was investigated by additional simulations at 4000 and 3000 K. The dissociation yields of each bond type across all three temperatures are presented in Figs. 13 and 14 for n-$C_4F_7H_3O$ and i-$C_4F_7H_3O$, respectively. As expected, the simulations at 5000 K produce the highest number of dissociation events of the three temperatures. However, a few exceptions to this trend appear primarily in the number of dissociated C—H bonds in n-$C_4F_7H_3O$ that peaks at 4000 K. This is a consequence of the lower number of the C—O bonds broken at a lower temperature, affording the opportunity for more C—H bonds to break from an unperturbed C#4. A similar effect occurs in i-$C_4F_7H_3O$, where the lower number of broken C—C bonds allows for more C—H and C—F bonds to be broken at 3000 K than at 4000 K. Interestingly, the initial fast kinetics of the dissociation, particularly of the C—O and the C—H bonds, are maintained to a certain extent across different temperatures, and overall, the fragmentation trends of the bond types are preserved.

Within the bond environments of n-$C_4F_7H_3O$, there are stronger and weaker temperature dependencies leading to a shifting of proportions of dissociations within each bond type. For the C—F bonds considered in Fig. 15, the C#3—F bond remains roughly contributing 50% of the total dissociation of the C—F bonds, further demonstrating the effect of oxygen. The other two environments dissociated at an approximately equal rate during the simulations at 5000 K, but as the temperature decreases, dissociations of the C#2—F bonds account for 42% of the dissociation of the C—F bonds at 3000 K. As the temperature decreases, the C—F bonds dissociate increasingly rarely, with the C#3—F environment breaking only a total of two times across all 400 trajectories at 3000 K. Therefore, it can be said that the dissociations of the C—F bonds broken for both the C#1—F and C#2—F environments at 3000 K can be almost entirely attributed to the effect of the oxygen atom.

Similarly, Fig. 16 shows that the C—O bond dissociations that were approximately equally distributed in n-$C_4F_7H_3O$ at 5000 K display a slight redistribution as the temperature decreases, as the dissociation of the C#4—O bond accounts for 59% of the C—O bonds dissociated across all trajectories for n-$C_4F_7H_3O$ at 3000 K. This can be explained by the reduced number of C—H bond dissociations than the simulations at 5000 K, which could have previously been curtailing the number of C#4—O bonds dissociated at higher temperatures, due to the C—H bonds often dissociating

29 May 2025 13:06:07

© Author(s) 2025

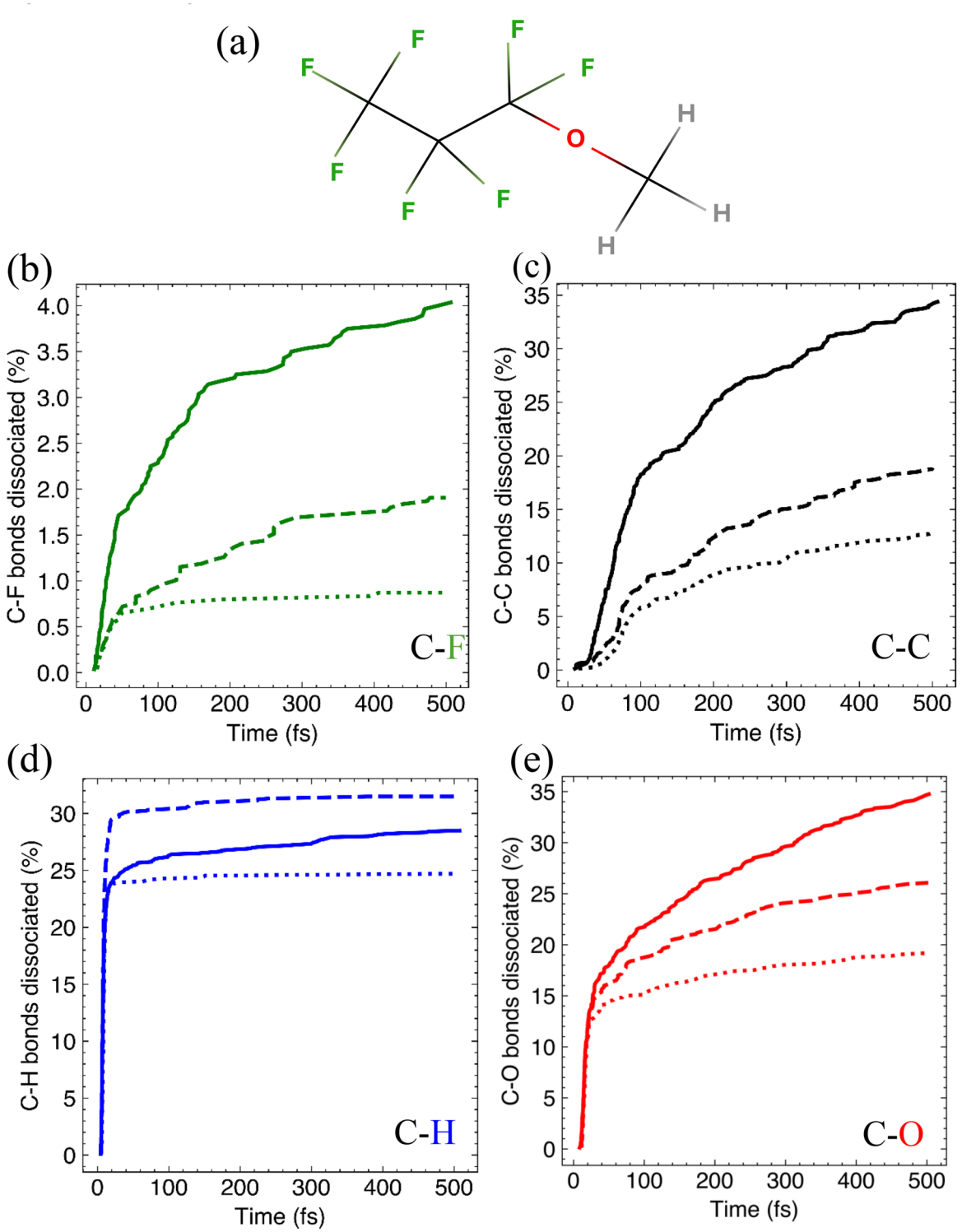

FIG. 13. (a) Molecular structure of n-$C_4F_7H_3O$ and the temperature dependence of the dissociation kinetics for (b) C—F, (c) C—C, (d) C—H, (e) C—O bonds. Three temperatures, 3000 K (dotted line), 4000 K (dashed line), and 5000 K (solid line) are compared.

29 May 2025 13:06:07

© Author(s) 2025

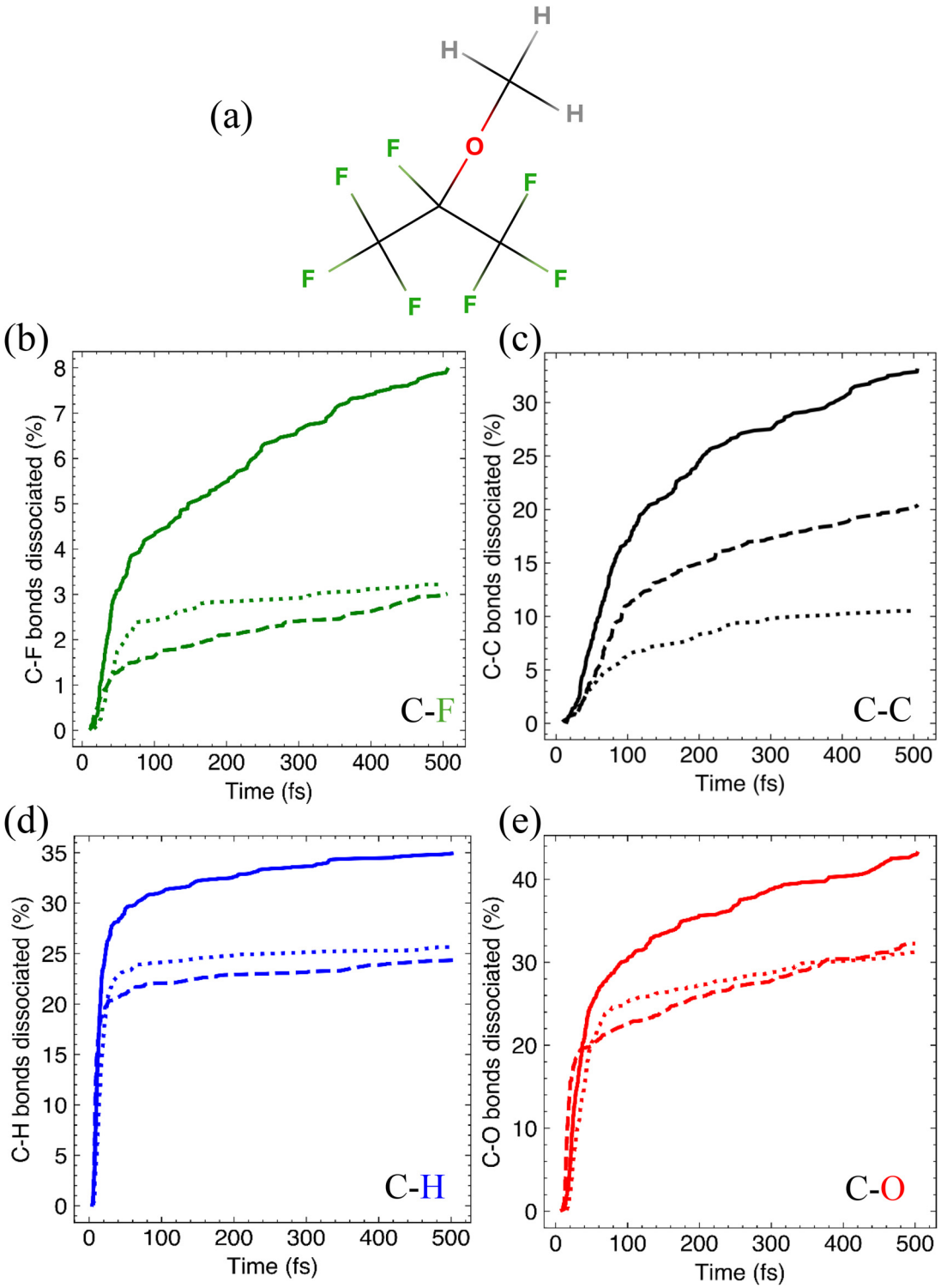

FIG. 14. (a) Molecular structure of i-$C_4F_7H_3O$ and the temperature dependence of the dissociation kinetics for (b) C—F, (c) C—C, (d) C—H, (e) C—O bonds. Three temperatures, 3000 K (dotted line), 4000 K (dashed line), and 5000 K (solid line) are compared.

29 May 2025 13:06:07

© Author(s) 2025

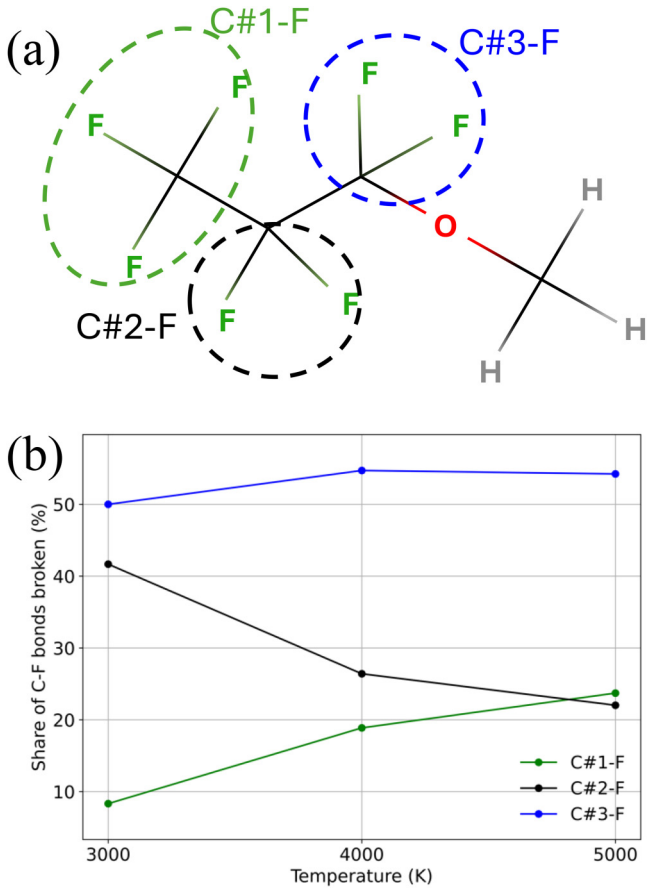

FIG. 15. (a) Molecular structure of *n*-$C_4F_7H_3O$ highlighting the different C—F environments, C#1—F (green, highest at T = 3000 K), C#2—F (black, 2nd highest at T = 3000 K), and C#3-F (blue, lowest at T = 3000 K) and (b) the temperature dependence of the dissociation kinetics for different C—F environments in the n—$C_4F_7H_3O$ molecule. The plot shows the number of broken C—F bonds in each environment as a percentage of all C—F bonds broken at that temperature.

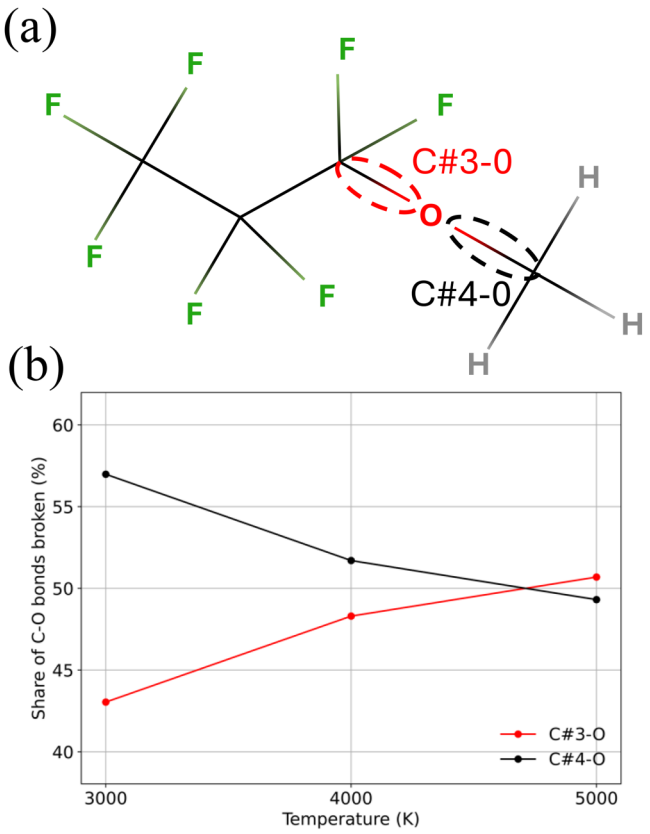

FIG. 16. (a) Molecular structure of n-$C_4F_7H_3O$ highlighting the different C-O environments, C#3—O (red, lowest at T = 3000 K), and C#4—O (black, highest at T = 3000 K) and (b) the temperature dependence of the dissociation kinetics for different C—O environments in the n—$C_4F_7H_3O$ molecule. The plot shows the number of broken C—O bonds in each environment as a percentage of all C—O bonds broken at that temperature.

rapidly at the beginning of simulations. The C—C bonds considered in Fig. 17 display a simple pattern, where the trend that the C#2—C#3 bond accounts for more of the C—C dissociations than the C#1—C#2 bond becomes more and more marked. This is because, at lower temperatures, the bonds are less likely to dissociate and so the deterministic effect of the oxygen atom plays an even larger role in determining the dissociation pathways.

The distribution of C—F dissociations across different environments shifts significantly as the temperature is varied in i-$C_4F_7H_3O$, as shown in Fig. 18. The steric effect of the methyl group at 5000 K is maintained across all temperatures due to the simulations beginning from the same optimized geometry, meaning that the C#1—F environment is responsible for more of the C—F dissociations than the C#3—F environment across all temperatures. As previously presented in Fig. 12, the C#2—F bond is the singular C—F bond that has the highest dissociation yield. However, since C#2—F contains only one bond, the C#1—F environment accounts for the largest proportion of C—F bonds broken at 5000 K. As the temperature decreases and the effect of the electrophore becomes more prevalent, the C#2—F environment continues to increase in the share of the total C—F bonds until at 3000 K, where the singular C#2—F bond dissociates more than the cumulative three bonds in the C#1—F environment.

The distribution of C—O dissociations across the C—O environments presented in Fig. 19 shows an interesting trend. The proportion of dissociations between the two C—O environments in i-$C_4F_7H_3O$ shifts toward an almost equal split at 4000 K, before returning to favoring the C#2—O bond accounting for 66% of all C—O bonds broken at 3000 K. This could be due to fluctuations in how the other bonds dissociate, as well as the dissociations of the two C—O bonds having different temperature dependences. Figure 13 shows that at 4000 K, the number of dissociations of both C—O bonds drops, with C#2—O dropping more, possibly due to the lower number of the C—H bonds broken, favoring the C#4—O

29 May 2025 13:06:07

© Author(s) 2025

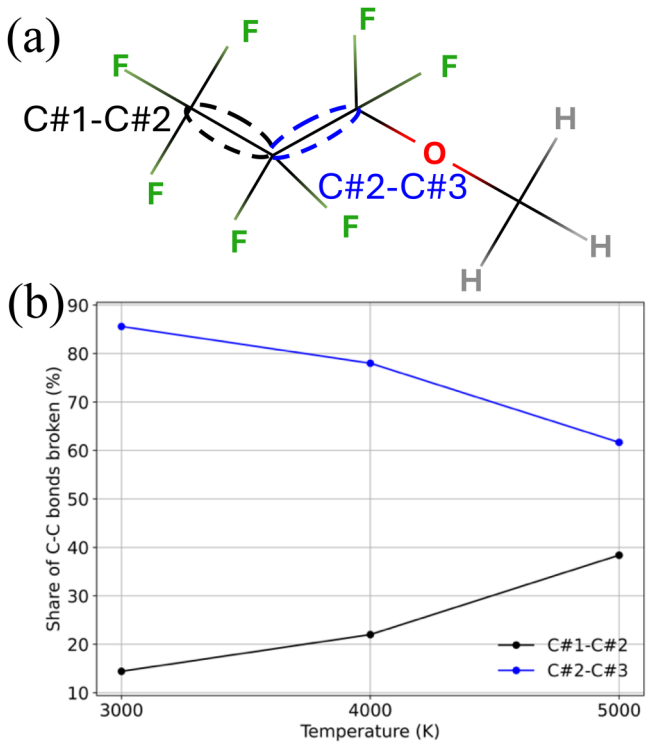

FIG. 17. (a) Molecular structure of n-$C_4F_7H_3O$ highlighting the different C—C environments, C#1—C#2 (black, lowest at T = 3000 K), and C#2—C#3 (blue, highest at T = 3000 K) and (b) the temperature dependence of the dissociation kinetics for different C-C environments in the n—$C_4F_7H_3O$ molecule. The plot shows the number of broken C—C bonds in each environment as a percentage of all C—C bonds broken at that temperature.

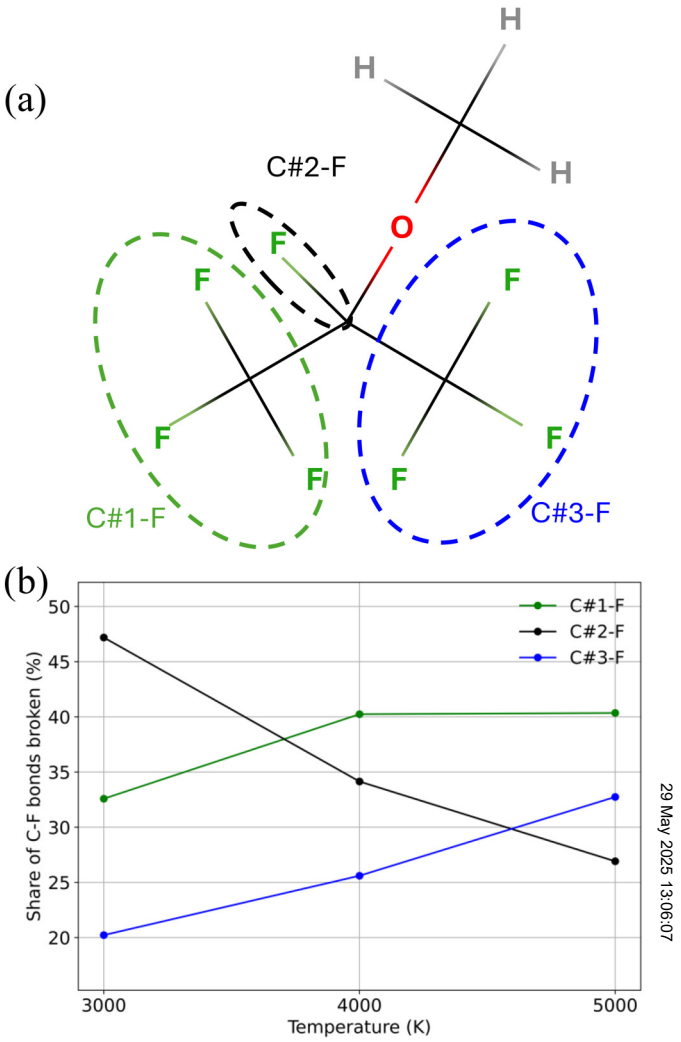

FIG. 18. (a) Molecular structure of i-$C_4F_7H_3O$ highlighting the different C—F environments, C#1—F (green, 2nd highest at T = 3000 K), C#2—F (black, highest at T = 3000 K), and C#3—F (blue, lowest at T = 3000 K) and (b) the temperature dependence of the dissociation kinetics for different C—F environments in the i-$C_4F_7H_3O$ molecule. The plot shows the number of broken C—F bonds in each environment as a percentage of all C—F bonds broken at that temperature.

bond. However, at 3000 K, the proportion of the C—O bonds of C#2—O increases when compared to 4000 K, likely due to the much lower dissociation yield of the C—C and C—F bonds, while C#4—O has a more expected temperature dependence.

6. Comparison with experiments

When these molecules were investigated experimentally to test whether they would be viable replacements for the C_4F_8 plasma precursor,[42,43] several key bonds were identified to be prominent in their neutral dissociation pathways. These highlighted bonds are displayed by dashed lines in Fig. 20; they correspond to the bonds most often dissociated in our simulations. For n-$C_4H_3F_7O$, the highlighted C—C bond is the C#2—C#3 bond, which we find to be the most broken C—C bond; see Fig. 9. Likewise, our simulation of the dissociation of n-$C_4H_3F_7O$ also showed the C—O bonds to be predominantly broken. For the case of i-$C_4H_3F_7O$, we also identify the C#2—O bond as the most broken as evidenced in Fig. 10, followed by both C—C bonds, roughly symmetrically. In the mass-spectrometry performed for both molecules, several major peaks were noted, namely, CF_3 and CH_3, with the addition of C_2F_5 for n-$C_4H_3F_7O$. At the lower temperatures of 3000 and 4000 K, the most common fragment in our simulations after atomic H is the molecule with only one hydrogen dissociated due to the lower number of total dissociations, followed by C_2F_5 and CH_3, agreeing well with the highlighted fragments from the experiment.

In our simulations of i-$C_4H_3F_7O$ at both 5000 and 4000 K, CF_3 was the most common radical produced after atomic H. For our simulations of n-$C_4H_3F_7O$ at 5000 K, C_2F_5 is the fourth most common final fragment, with CF_2 being the second most common fragment after atomic H. The fact that the fragment CF_2 is more common than CF_3 is a consequence of the fact that the simulations were performed at 5000 K, leading to excess fragmentation. The authors of

29 May 2025 13:06:07

© Author(s) 2025

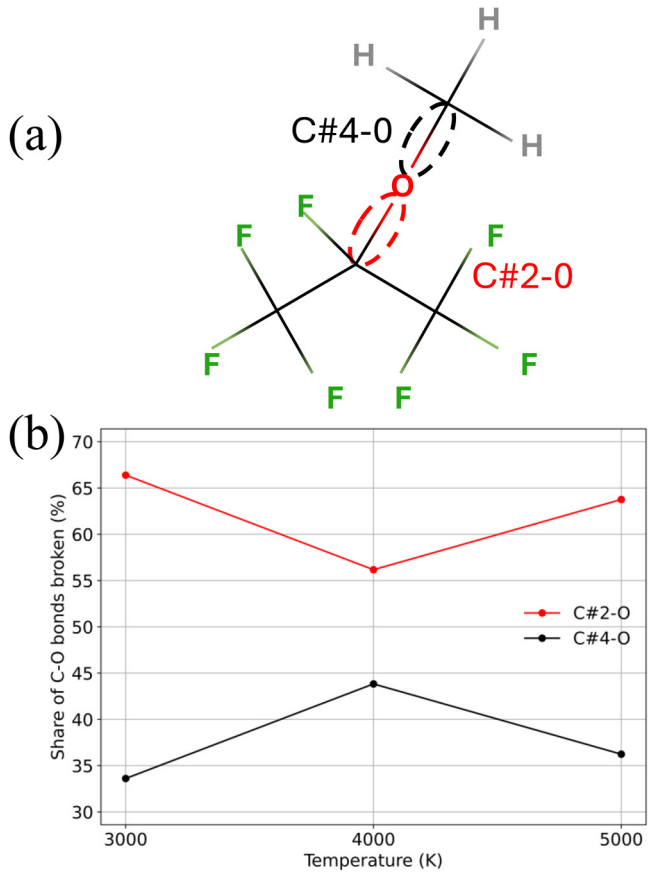

FIG. 19. (a) Molecular structure of i-$C_4F_7H_3O$ highlighting the different C—O environments, C#2—O (red, highest at T = 3000 K), and C#4—O (black, lowest at T = 3000 K) and (b) the temperature dependence of the dissociation kinetics for different C—O environments in the i-$C_4F_7H_3O$ molecule. The plot shows the number of broken C—O bonds in each environment as a percentage of all C—O bonds broken at that temperature.

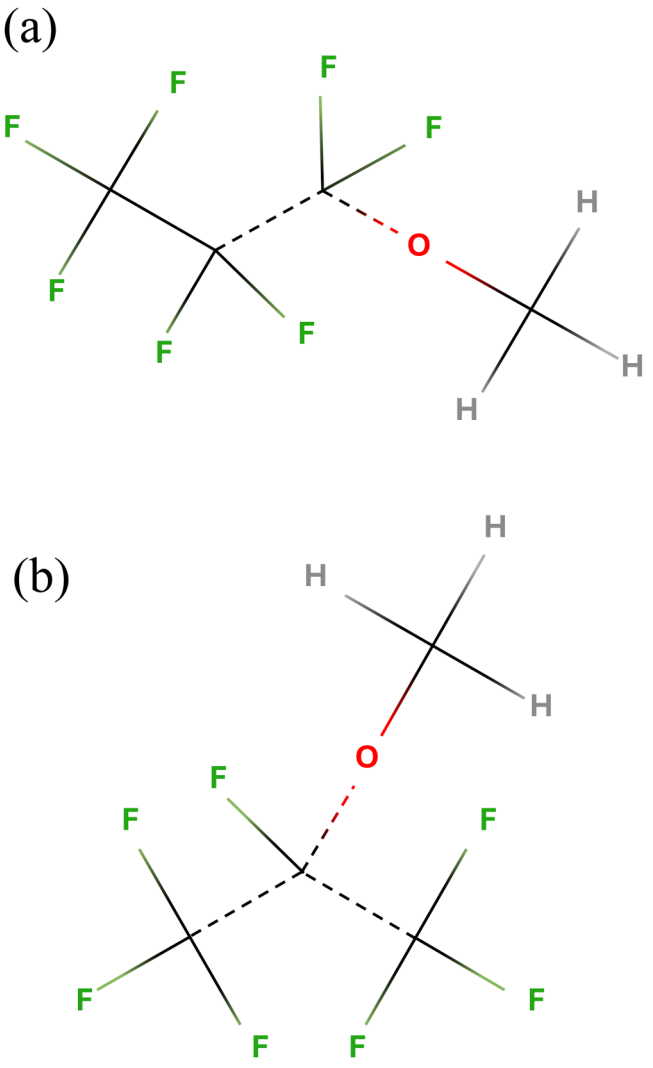

FIG. 20. Recreation of structural diagrams for both (a) n-$C_4H_3F_7O$ and (b) i-$C_4H_3F_7O$ shown in Fig. 2 of Ref. 24. The bonds that were highlighted to be prone to dissociation have been replaced with dashed lines.

the experimental paper[43] attribute weakening of the C—C bonds to the presence of the methoxy group and its electron-withdrawing effect. In addition, we detail the role oxygen lone pairs play in the formation of the triplet state of the methoxy group.

The results presented for both n-$C_4H_3F_7O$ and i-$C_4H_3F_7O$ can be explained by our "electrophore" model presented in Sec. II A. The oxygen atom provides an initial triplet state localization due to the lone pairs of the oxygen atom having a small energy gap to the lone pair orbital and antibonding orbital of the CO bonds. The population of this antibonding orbital then accounts for the higher number of dissociations of the C—O bonds. This electronic and spin density can then be donated to the surrounding bonds, causing the C#2—C#3 bond to dissociate more than the C#1—C#2 bond in n-$C_4H_3F_7O$. This can also be seen in the C—F bonds in both isomers, as the C—F bonds that dissociate the most are the ones closest to the oxygen atom and can, therefore, more readily accept the dissociative character of the triplet state localization. The central oxygen in i-$C_4H_3F_7O$ is closer to more atoms and, therefore, can donate its antibonding characteristics to multiple different places, leading to the overall higher number of dissociations seen for this molecule than for n-$C_4H_3F_7O$.

B. Dissociation pathways in $C_4F_7H_2OH$

1. Overall behavior

The electronic excitation cross sections for $C_4F_7H_2OH$ shown in Fig. 21 demonstrate that the lowest excited state is a triplet state. Although the second lowest state is a singlet state, excitation of the lowest triplet is, in fact, dominant throughout the whole energy range considered, supporting the assumption of only the lowest triplet state being vital for dynamics. For $C_4F_7H_2OH$, the O—H

29 May 2025 13:06:07

© Author(s) 2025

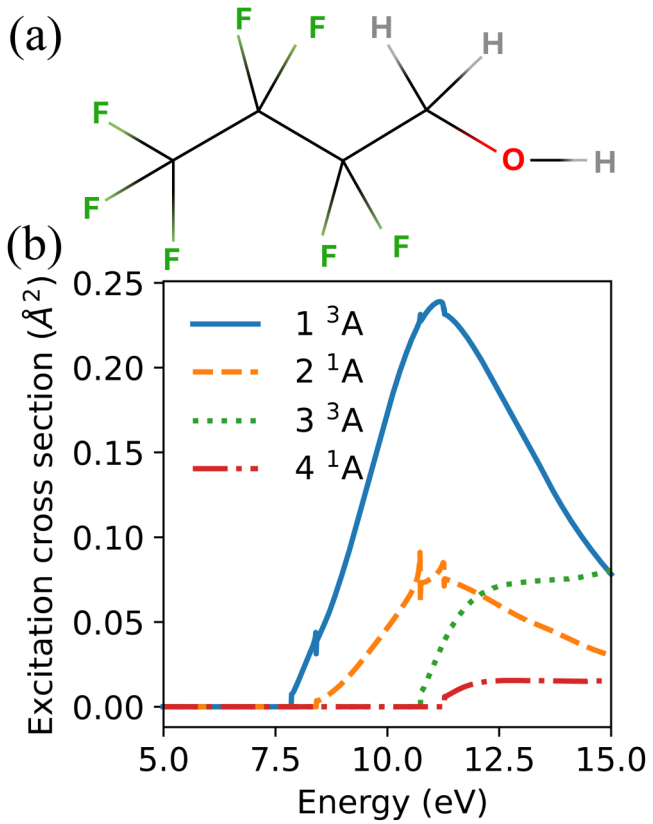

FIG. 21. (a) Molecular structure of $C_4F_7H_2OH$ with its (b) electron impact excitation cross sections calculated using QEC.

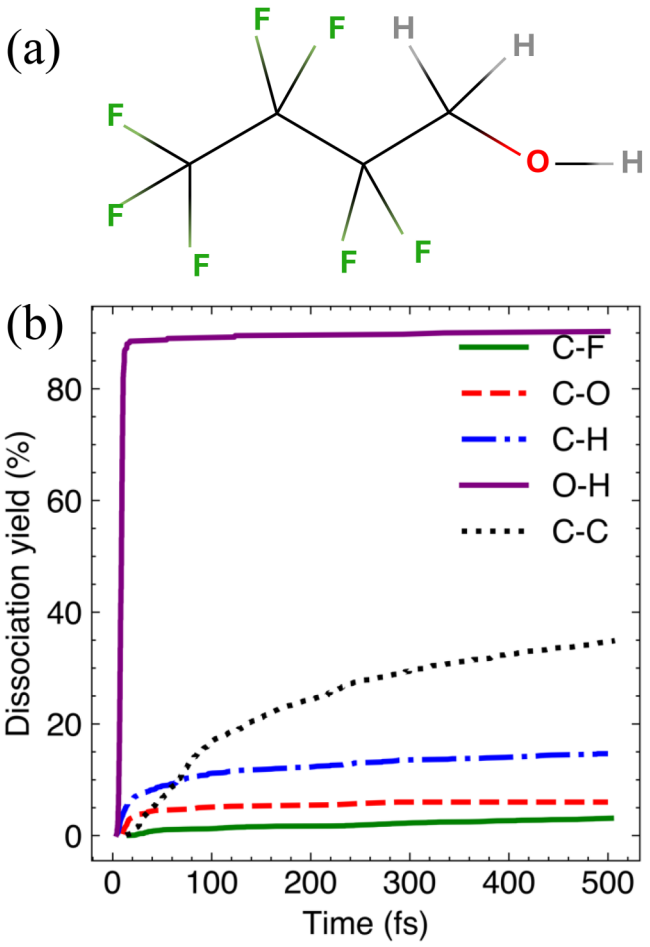

FIG. 22. (a) Molecular structure of $C_4F_7H_2OH$ and (b) the comparison of the dissociation kinetics for its different bonds at 5000 K.

bond dominates the dissociation pathways with a 90% dissociation yield, as shown in Fig. 22. As alcohol contains only one O—H bond, this bond breaks in 90% of the trajectories and is the first bond broken in 86% of them, accounting for 33% of the total bonds dissociating in the molecule. The C—C bonds in this molecule have a dissociation yield of 35%, meaning that, on average, at least one C—C bond breaks per trajectory, as $C_4F_7H_2OH$ contains three C—C bonds. Interestingly, the C—O dissociation behavior in this molecule is completely different from that observed previously for the other isomers of $C_4H_3F_7O$, with a dissociation yield of 6%, with not a single C—O bond broken after 300 fs. The C—H bonds also present a much lower dissociation yield than the previous isomers with only 15% of the C—H bonds dissociating. The position of these C—H bonds combined with the functional group of the oxygen atom can explain the low breaking of the C—O bond, as the majority of the C—H bonds dissociate within 100 fs, meaning that after the dissociation of the C—H and O—H bonds, both the carbon and oxygen atoms that form the C—O bond have already lost a bond, heavily discouraging dissociation. The C—F bonds also give the lowest average across the three isomers, having a dissociation yield of 3.1%. This lower amount can be explained by the fact that no fluorine atoms are bonded to C#4 of the molecule, which is the only carbon adjacent to the oxygen atom, therefore, diminishing the electrophoric effect of the oxygen atom.

As previously mentioned, the neutral dissociation pathways of the $C_4F_7H_2OH$ molecule are clearly dominated by the dissociation of the O—H bond, being the first dissociation event most often with an average occurrence time of 8.5 fs. This also provides an explanation as to why the breaking behavior for the C—O bond in the alcohol isomer is the opposite of that found in the other molecules studied, as the oxygen atom is discouraged from breaking a second bond, as it is already a radical. While the oxygen bonds are clearly breaking in one direction, the secondary effect of the weakening adjacent bonds is still visible when comparing the breaking patterns within the C—C and C—F groups, presented in Figs. 23 and 24.

2. C–C and C–F bonds

The C#3—C#4 bond breaks more often than both other C—C bonds combined, shown in Fig. 23, accounting for 55% of the

29 May 2025 13:06:07

© Author(s) 2025

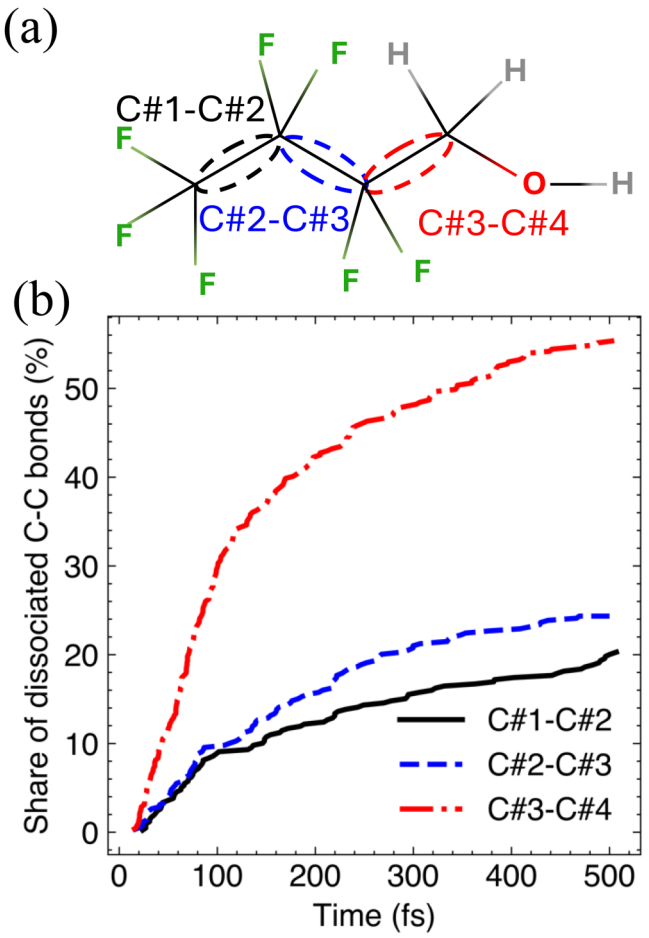

FIG. 23. (a) Molecular structure of $C_4F_7H_2OH$ highlighting the different C—C environments, C#1-C#2 (black solid line), C#2—C#3 (blue dashed line), and C#3—C#4 (red dashed–dotted line) and (b) the comparison of the dissociation kinetics for different C—C bonds in $C_4F_7H_2OH$ at 5000 K. The average number of dissociations per bond in each environment is shown as a percentage of the total number of C—C bond dissociations for 500 fs.

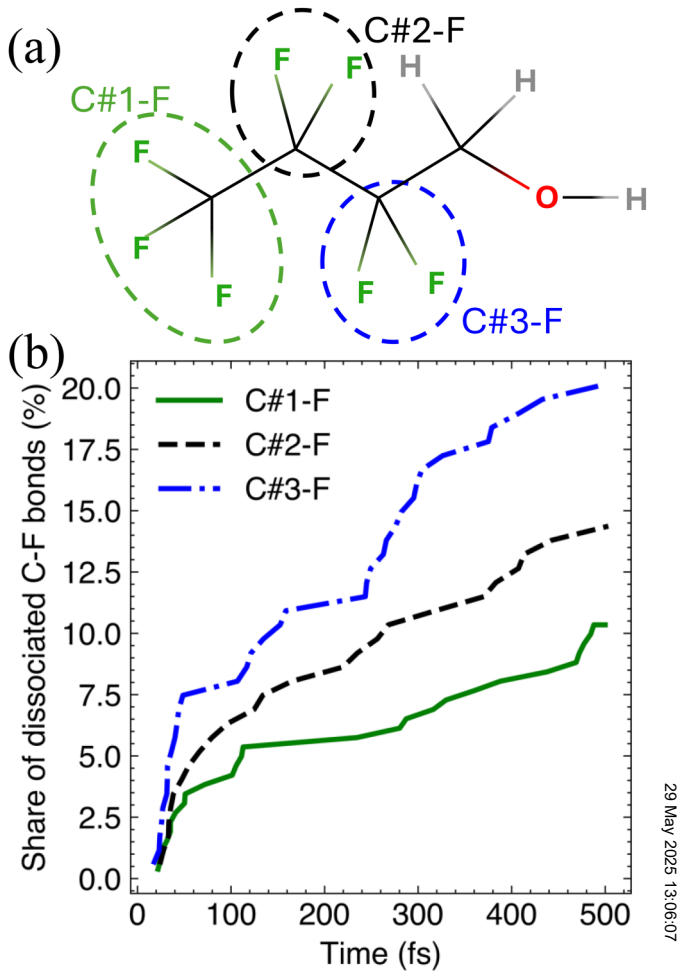

FIG. 24. (a) Molecular structure of $C_4F_7H_2OH$ highlighting the different C—F environments, C#1—F (green solid line), C#2—F (black dashed line), and C#3—F (blue dashed–dotted line) and (b) the comparison of the dissociation kinetics for different C—F bonds in $C_4F_7H_2OH$ at 5000 K. The average number of dissociations per bond in each environment is shown as a percentage of the total number of C—F bond dissociations for 500 fs.

C—C bonds broken in $C_4F_7H_2OH$. This C—C bond breaks significantly more than all C—C bonds considered for the other $C_4F_7H_3O$ isomers in Figs. 9 and 10. This is because it is the only C—C bond adjacent to the electrophoric oxygen atom and that the C—O bond almost never breaks due to the very dissociative O—H bond. The difference in dissociation yield between C#2—C#3 and C#1—C#2 is less pronounced as both bonds are a further distance from the oxygen atom and, therefore, are weakened by an increasingly reduced amount but still maintain the order of the number of dissociations being proportional to the distance to the oxygen atom, with a proportion of the C—C bonds broken of 25% and 20%, respectively.

Breakage of the C—F bonds (shown in Fig. 24) also demonstrates a dependence on the distance between the C—F environments and the oxygen atom. This effect is, however, less noticeable than for the C—C bonds, explained by the fact that there are no C—F bonds on the carbon bonded to the oxygen atom. The C#1—F and C#2—F environments account fairly equally for the C—F bond breaking. However, the C—F bonds within the C#2—F environment can be considered to be more efficient due to the fewer number of bonds in the environment, as each of the two bonds in the C#2—F environment accounts for 14% of the C—F dissociations in $C_4F_7H_2OH$. Each bond in the C#2—F environment has a dissociation yield of 3.1% compared to 2.3% for each of the three bonds in C#1—F, resulting in the efficiency of the C—F environments presented in Fig. 24. The C#3—F environment contains the C—F bonds closest to the oxygen atom, and so each of the C#3—F bond accounts for 20% of the overall C—F dissociations in

29 May 2025 13:06:07

© Author(s) 2025

$C_4F_7H_2OH$. The small number of C—F bonds broken in this molecule is a notable example of how, in order to gather details on pathways involving C—F dissociation, a large number of trajectories are often needed.

3. Temperature dependence

Breakage of different bonds in the alcohol isomer $C_4F_7H_2OH$ showcases different temperature dependence; see Fig. 25. First, the rate of O—H dissociations is almost completely indifferent to the temperature, suggesting that the O—H bond is so weak that the dissociation can be said to be barrierless and driven by the repulsive potential energy of the O—H bond in the triplet state even at 3000 K, where it accounts for over 60% of the total dissociations of the molecule. This weakness could be due to the fact that a small atom like H is bonded to the electrophore. The C—H bonds and the C—C bonds present with fairly similar behavior where the dissociation count for both bond types decreases as the temperature decreases, with the decrease being relatively more severe with lower temperatures.

The dissociation yield of the C—O bonds approximately halves when the temperature is reduced from 5000 to 3000 K, maintaining roughly an equal percentage of total bonds dissociated across all three temperatures considered. As the temperature decreases, the C—F bond breakings become practically nonexistent, with a total of three C—F bonds broken across all trajectories at 3000 K, all of which belong to the C#3—F environment, the closest to the oxygen atom. This further supports the idea that at lower temperatures like 3000 K, the C—F bonds only break due to interactions with the electrophore.

4. Comparison with experiments

$C_4F_7H_2OH$ was also investigated in the same paper as the other $C_4F_7H_3O$ isomers.[42] Interestingly, there are no specifically highlighted bonds for this molecule, which could be due to the fact that this molecule tends to have fewer dissociation events when compared to the other isomers. The authors of the experimental paper also reported that the n- and i-isomers decompose much more than the alcohol isomer, which agrees with our simulations which find significantly fewer dissociations than for the previously considered molecules. When comparing different mass spectra for each molecule found in Ref. 24, the CO peak in $C_4F_7H_2OH$ had a higher intensity than the CO peak present in the mass spectrum of ether isomers, which is corroborated by our theoretical findings that the C—O bond dissociates very infrequently in $C_4F_7H_2OH$. The C#2—C#3 bond and the O—H bond break very frequently, and as an atom is discouraged to experience a second bond dissociate, the C—O bond rarely dissociates, resulting in the CO radical observed.

Through the lens of the "electrophore" model presented in Sec. II A, when the lowest triplet state is initially populated via electron impact, the lone pairs on the oxygen atom cause it to act as an electrophore, localizing the spin density of the triplet state. Due to the excitation of the antibonding orbital, a weakening effect occurs, causing the bonds that contain the oxygen atom to be more likely to dissociate. As the hydrogen atom is very light, the O—H bond then dissociates very readily and rapidly. The antibonding character is also donated to the surrounding bonds, weakening the bonds close to the oxygen atom. This causes the C—H and the C#3—C#4 bonds to break significantly, while the bonds further away are less affected, with the number of dissociation events lowering further and further as the distance from the oxygen atom increases. This gives rise to the order of the dissociations of the C#2—C#3 bond breaking more than the C#1—C#2 bond and the order of the C—F environments of C#3—F, C#2—F, and C#1—F.

C. Dissociation pathways in PPVE

1. Overall behavior

The electron impact excitation cross sections for the PPVE molecule are shown in Fig. 26. For electron energies below 14 eV, the cross section is nonzero for only one excited state, which is a triplet. Interestingly, this excited state cross section appears at much lower energies than in the other molecules considered previously, with the triplet state emerging just after 6 eV. This value fits with the results found when the double C═C bond was investigated as an electrophore previously by our group,[4] showing that the triplet state behavior shown in Fig. 26 can be attributed to the C═C bond present in PPVE. PPVE is an interesting molecule as it contains both the C—O—C bonds present in $C_4H_3F_7O$ isomers as well as a double carbon—carbon bond that was deemed important in our previous paper on triplet state dissociation,[4] allowing us to determine the interaction between two important factors for determining the dissociation of a molecule.

When comparing the dissociation kinetics of the overall bond types in PPVE in Fig. 27, it is evident that the C—O bonds once again break very often, with a dissociation yield of 41%. Interestingly, despite the C═C bond being outnumbered by the C—C bonds 2 to 1, there are still marginally more C═C bonds breaking per trajectory than the C—C bonds with dissociations of 70% and 34%, respectively, suggesting that the C═C bond is broken much more efficiently. In the ground (singlet) state of a molecule, double C═C bonds are stronger than single C—C bonds but the PES of the same molecule in the excited triple state differs from that of the ground state, due to the repulsive nature of the "antibond" populated in the triplet state. The C—F bonds predictably give a low percentage of dissociation yield with just 5.4%, and here it is important to note that PPVE contains ten C—F bonds compared to i-$C_4H_3F_7O$ containing seven, meaning that PPVE is less efficient in terms of the number of C—F bonds broken in the molecule.

2. C–O bonds

As with most of the other molecules, the molecule is not symmetrical around the oxygen bond and so the averaged bond type graph is perhaps slightly misleading. The dissociation of PPVE heavily favors breaking the C#3—O bond that results in the oxygen radical containing the double carbon—carbon bond. Figure 28 shows that the difference between the C#3—O and the C#4—O bonds is rather drastic, with the C#3—O bond accounting for 80% of the C—O dissociations in PPVE, having a dissociation yield of 66%. This is by far the largest separation between two different oxygen containing bonds not including the alcohol group of

29 May 2025 13:06:07

© Author(s) 2025

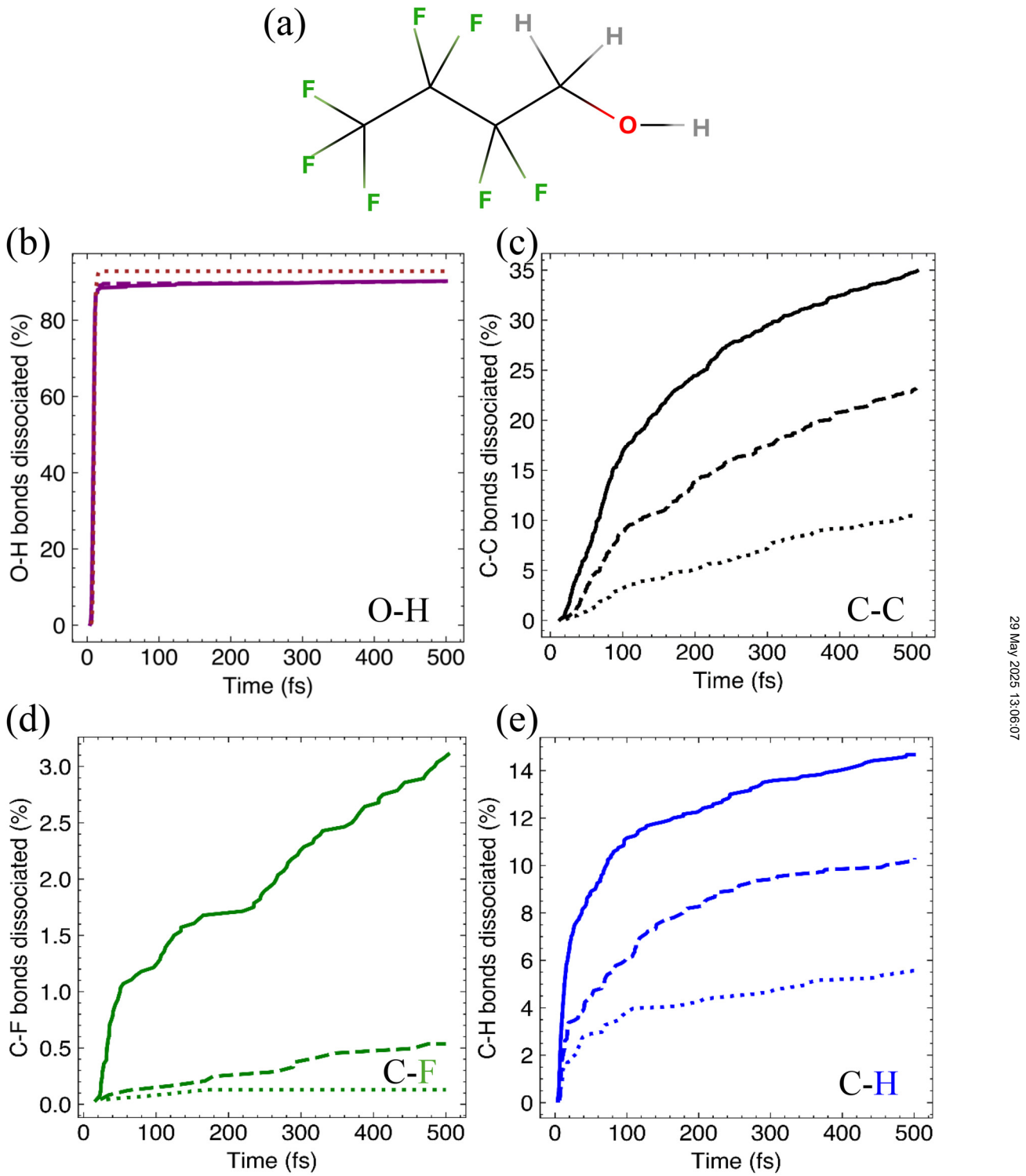

FIG. 25. (a) Molecular structure of $C_4F_7H_2OH$ and the temperature dependence of the dissociation kinetics for (b) O—H, (c) C—C, (d) C—F, (e) C—H bonds. Three temperatures, 3000 K (dotted line), 4000 K (dashed line), and 5000 K (solid line) are compared.

29 May 2025 13:06:07

© Author(s) 2025

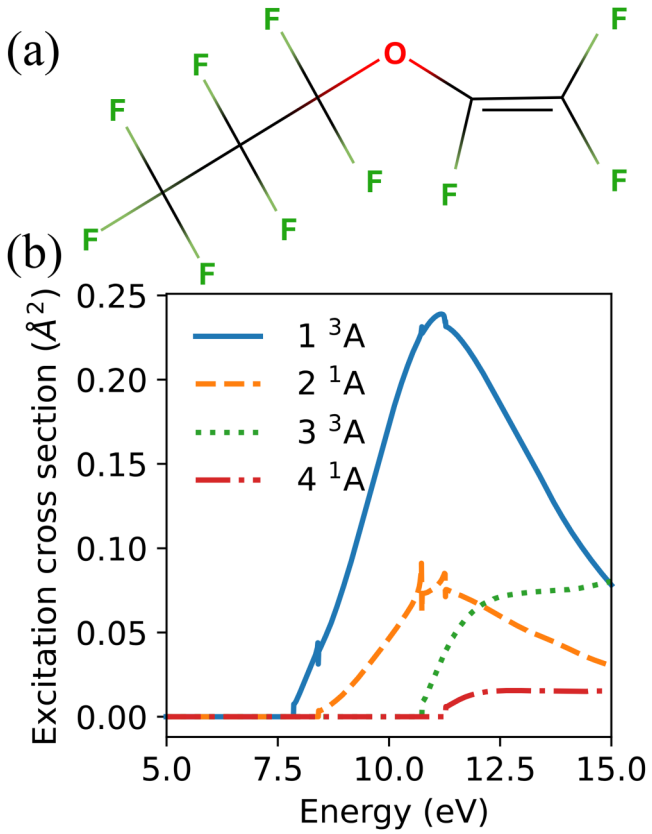

FIG. 26. (a) Molecular structure of PPVE with its (b) electron impact excitation cross sections calculated using QEC.

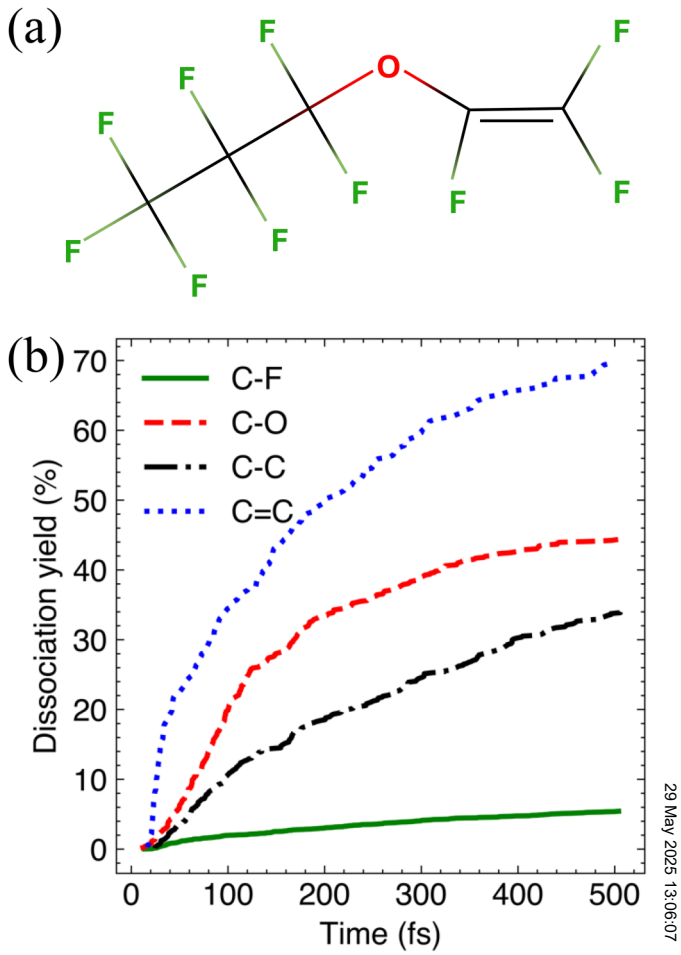

FIG. 27. (a) Molecular structure of PPVE with the (b) comparison of the dissociation kinetics for its different bond types at 5000 K.

$C_4F_7H_2OH$, which can be considered as a special case due to the different functional groups, suggesting that the double C═C bond plays a large role in influencing the C—O bond dissociation. The conditions that accelerate the dissociation of the C#3—O bond cause it to be the most broken, with this single bond accounting for 25.29% of all dissociations in PPVE at 5000 K.

3. C-C and C-F bonds

The effect of the oxygen atom and the carbon—carbon double bond can be seen not only in the bonds containing the oxygen atom breaking the most often, but also in the frequency of the dissociation of the neighboring bonds. The carbon—carbon bonds rupture, as in Fig. 29, show a simple clear picture that carbon closest to the oxygen bonds break over twice as fast with C#2—C#3 reporting a 41% dissociation yield compared to just 23% of C#1—C#2. Therefore, the C—C bond involving carbon furthest from oxygen dissociates significantly more, with C#2—C#3 accounting for 60% of the C—C dissociations in PPVE at 5000 K. The dissociation of the C#2—C#3 bond also occurs after the dissociation of the C#3—O bond 53.7% of the time, meaning that the C#2—C#3 bond is dissociative to the extent that dissociation can occur after the breaking of another bond on the same carbon.

In the context of the C—F bonds shown in Fig. 30, the C—F bond that is formed with carbon that experiences the bond to both oxygen and carbon with a double bond clearly dominates the C—F dissociation events, with 56% of C—F dissociations being the C#4—F bond, dissociating more times than every other C—F bond combined. The only C—F environment apart from the C#4—F bond that has a notable dissociation yield is the C#5—F environment which experiences the electrophoric effect of the double bond. The other environments are generally indistinguishable and occupy a negligible proportion of the C—F bond dissociations. When averaged by the number of bonds per environment, all C—F environments in PVPE fall into the order of closer to the oxygen atom and the double bond having a higher number of bond breakages. As most of the dissociations for all bond types occur around oxygen and the double bond, this can be considered the "active" region of the molecule.

29 May 2025 13:06:07

© Author(s) 2025

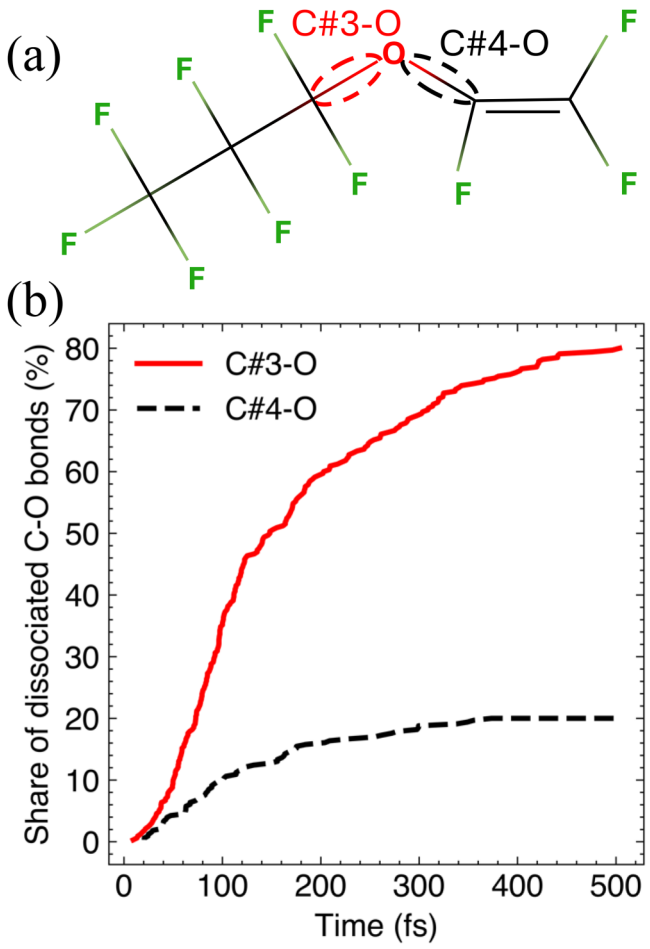

FIG. 28. (a) Molecular structure of PPVE highlighting the different C—O environments, C#3—O (red solid line), and C#4—O (black dashed line) and (b) the comparison of the dissociation kinetics for different C—O bonds in PPVE at 5000 K. The average number of dissociations per bond in each environment is shown as a percentage of the total number of C—O bond dissociations for 500 fs.

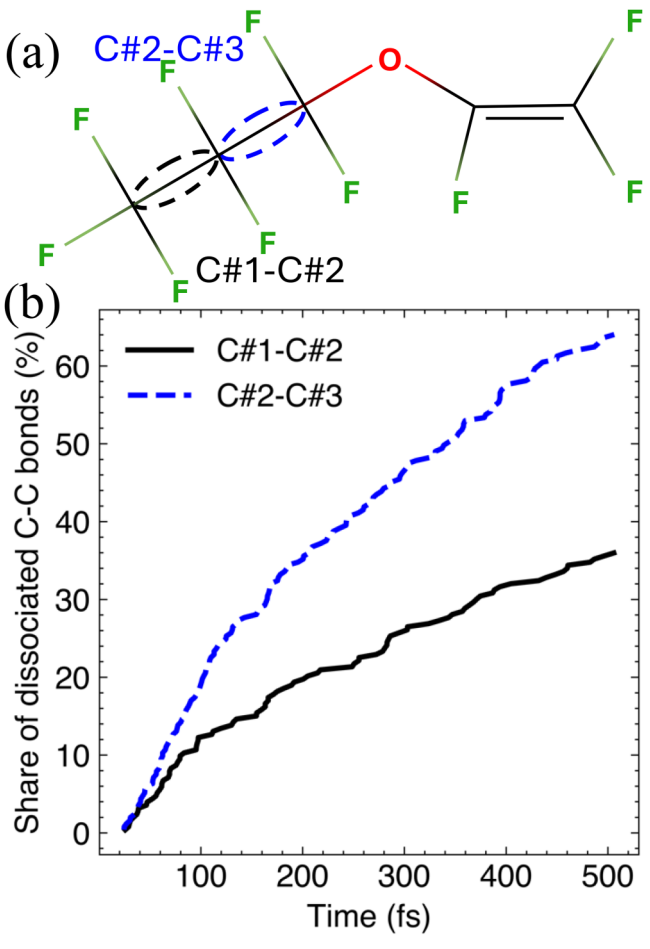

FIG. 29. (a) Molecular structure of PPVE highlighting the different C—C environments, C#1—C#2 (black solid line), and C#2—C#3 (blue dashed line) and (b) the comparison of the dissociation kinetics for different C—C bonds in PPVE at 5000 K. The average number of dissociations per bond in each environment is shown as a percentage of the total number of C—C bond dissociations for 500 fs.

4. Further details

Analyzing the order in which the bonds are broken, it is possible to gather a picture of dissociation routes. In general, a bond break discourages the subsequent bonds breaking; in this case, for the same carbon. This can be seen by studying the "active region" of PPVE, where, for example, both C—O bonds break only one time across all our calculations for PPVE at 5000 K. When the C#3-O bond breaks, the most common next broken bond is the C═C bond at 38.4% of the time. However, when the C#4-O bond breaks, the most common next broken bond is C#2—C#3 at 46.38% while the C═C bond is the next broken bond only 7.25% of the time, as C#4 carbon has already experienced a dissociation event. The double bond breaking also encourages the C#3—O bond to break subsequently over the C#4—O bond at 32.77% versus 8.94%. We theorize that the tendency for the same atom not to experience multiple bond breaks is the reason why the fluorine atoms on C#3 experience bond breaking behavior more similar to the C—F bonds further away from oxygen, as opposed to the C#4—F or C#5—F environments.

Conversely, the extent to which the C#4—F bond breaks is exemplary of how the effects of oxygen and the double bond are additive. In trajectories where the C#3—O bond breaks (which itself occurs in 70% of all trajectories), the C#4—F bond breaks afterward 29% of the time, meaning this dissociation pathway occurs in 20% of all trajectories and is, in fact, the third most common dissociation pathway undertaken by the molecule. As expected, when the opposite C—O bond breaks (C#4—O), C#4—F is discouraged from breaking afterward and this dissociation

29 May 2025 13:06:07

© Author(s) 2025

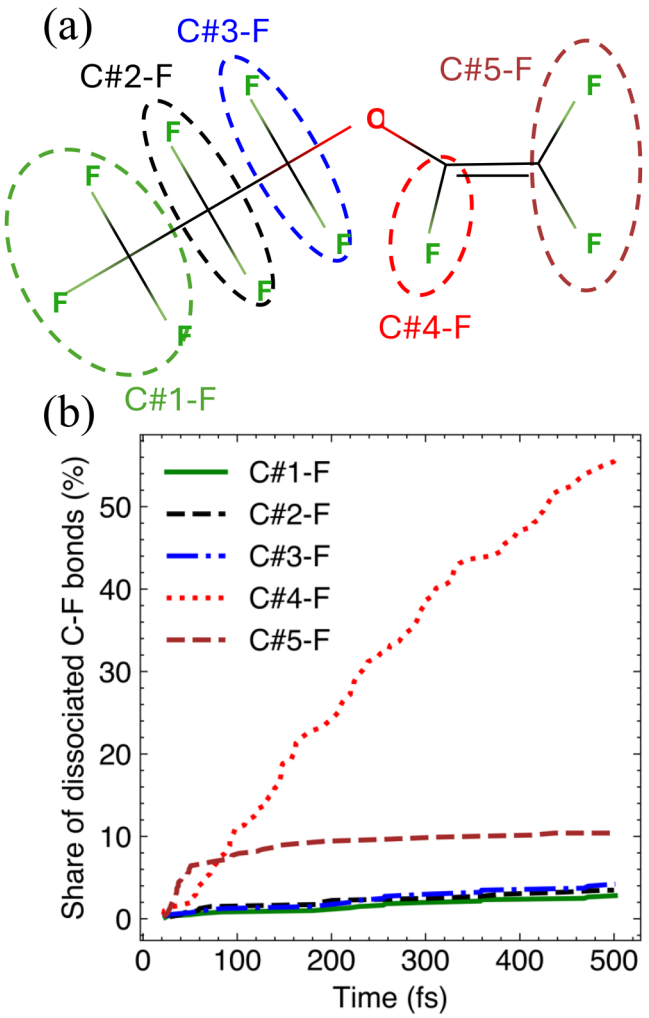

FIG. 30. (a) Molecular structure of PPVE highlighting the different C—F environments, C#1—F (green solid lines), C#2—F (black dashed line), C#3—F (blue dotted line), C#4—F (red dotted line), and C#5—F (brown dashed line) and (b) the comparison of the dissociation kinetics for different C—F bonds in PPVE at 5000 K. The average number of dissociations per bond in each environment is shown as a percentage of the total number of C—F bond dissociations for 500 fs.

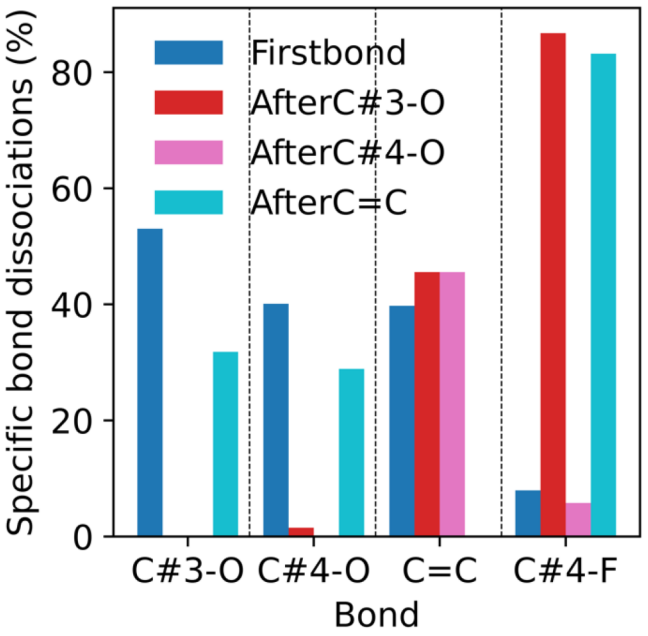

FIG. 31. Proportions of the conditions under which the bonds in the "active region" of PPVE dissociate. Each bar shows the percentage of the bond that breaks before others in the "active region" (dark blue, first bar), after the C#3-O bond (red, second bar), after C#4-O (pink, third bar), or after the C=C bond (light blue, fourth bar).

pathway only occurs three times in 400 trajectories, accounting for only 2.7% of all C#4—F breaking. The interesting data is that the breaking of the C═C bond does not equally discourage the breaking of the C#4-F bond as it is the next broken bond 26% of the time. The C#4—F bond is only broken as the first bond 10 times of the total 173 times the bond is broken throughout all trajectories meaning that it breaks after another bond is broken over 95% of the time.

Interestingly, the C#4-F bond seems to predominantly break after the dissociation of the C═C or C#3—O bonds, a significant 80% of the C#4—F bonds are broken after both C═C and C#3-O. This can also be seen with the average time of dissociation as C═C, C#3—O, and C#4—O all have similar averages of 146, 152, and 132 fs, respectively, whereas the average time for breaking of the C#4—F bond is 237 fs. The other bonds considered in the "active region" in Fig. 31 have a significant proportion of breaking where they are the first bond dissociated in the simulation and apart from the C═C bond, the C#4—O bond when broken discourages breaking of all other bonds in the active region. It is interesting to note that while C#3-O is the bond that most often breaks first in the trajectory, C═C breaks first quicker with an average breaking time of 51 fs vs 131 fs.

5. Temperature dependence

Investigating the temperature dependence of the active region of PPVE shows different interesting trends in Fig. 32. The decrease in temperature has the expected effect on the C#4—F bond, which is that it reduces from a dissociation yield of 28% at 5000 K to 18% at 4000 K to just 6% at 3000 K. A similar pattern can be seen in the C═C and both C—O bonds, where the average number of bonds dissociated decreases when the temperature decreases from 5000 to 4000 K and then decreases by a larger proportion when the temperature is decreased again to 3000 K. While the general pattern of temperature dependence is equivalent for all bond types, the amount by which their dissociation yield decreases shows that the extent of the temperature dependence varies. The most interesting

29 May 2025 13:06:07

© Author(s) 2025

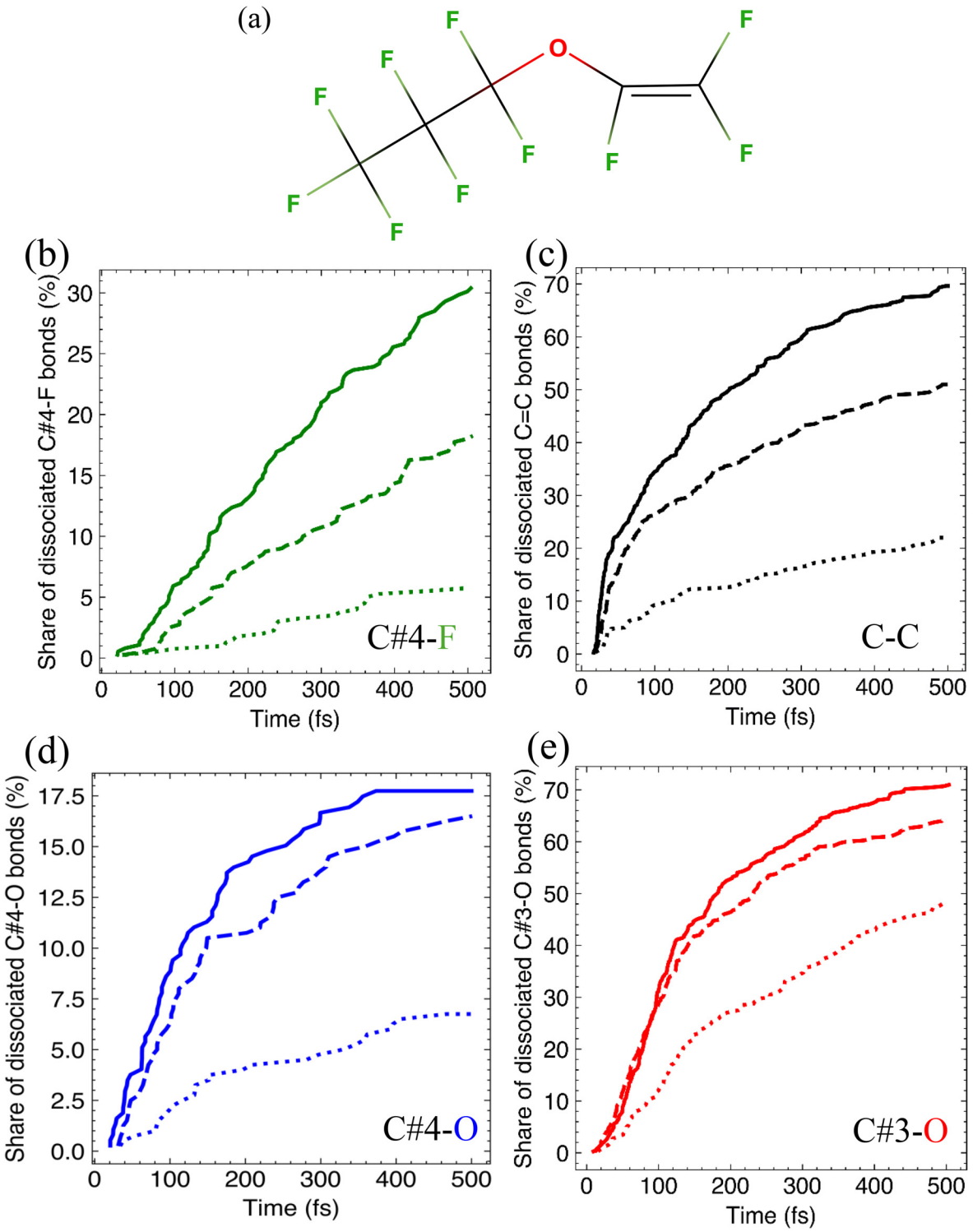

FIG. 32. (a) Molecular structure of PPVE and the temperature dependence of the dissociation kinetics for (b) C#4—F, (c) C═C, (d) C#4—O, (e) C#3—O bonds. Three temperatures, 3000 K (dotted line), 4000 K (dashed line), and 5000 K (solid line) are compared.

29 May 2025 13:06:07

© Author(s) 2025

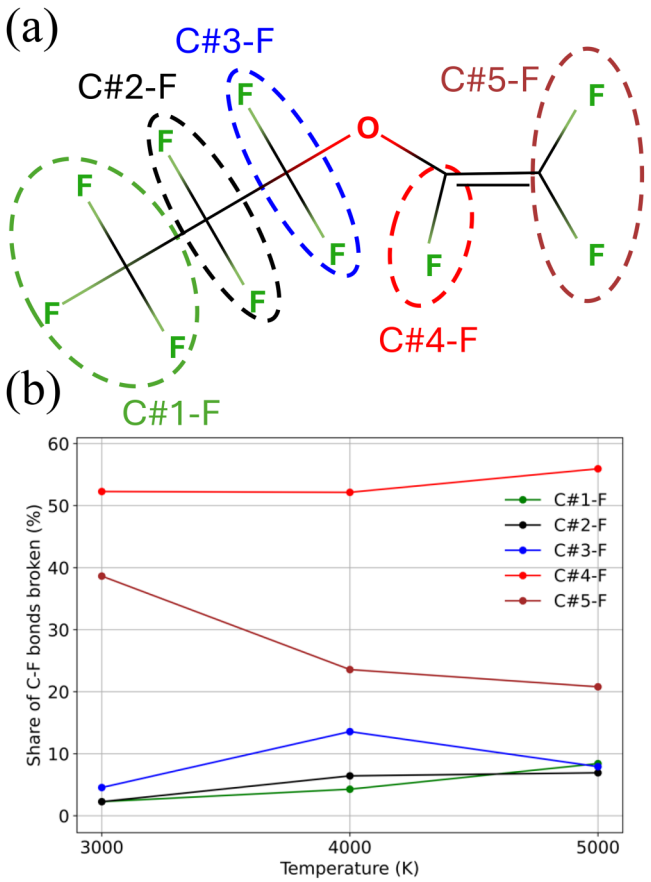

FIG. 33. (a) Molecular structure of PPVE highlighting the different C—F environments, C#1—F (green, lowest at T = 4000 K), C#2—F (black, 4th highest at T = 4000 K), C#3—F (blue, 3rd highest at T = 4000 K), C#4—F (red, highest at T = 4000 K), and C#5—F (brown, 2nd highest at T = 4000 K) and (b) the temperature dependence of the individual C—F environments for PPVE. Each C—F environment is assigned the percentage of all C—F bonds broken at that temperature.

case for this in PPVE is that of the C#3—O bond, which decreases proportionally the least and, as such, the percentage of total bond dissociations being the C#3—O bond increasing as the temperature is lowered until at 3000 K, almost 50% of all PPVE bonds broken are the C#3—O bond.

For both the C—C and C—O bonds in PPVE, the proportion between the different individual environments for each bond type is maintained across different temperatures. Figure 33 shows that while the exact distribution of dissociations across the different C—F environments changes as the temperature varies, the order of dissociation is maintained. Interestingly, when the temperature decreases to 4000 K, the proportion of C—F dissociations being the dissociation of a C#3—F bond increases. This supports our theory proposed in the explanation of Fig. 30 that the high number of C#1—C#2 and C#3—O dissociations was a limiting factor for the dissociation of the C#3—F bonds. At 3000 K, it is difficult for any C—F bond to dissociate and, therefore, the only C—F bonds with any significant number of dissociations are those around the C═C bond, namely, the C#4—F and C#5—F bonds. Across all temperatures, it remains clear that the electrophoric effects of the oxygen atom and the C═C bond are cumulative as the average number of dissociations is higher for the singular C#4—F bond than for both the C#5—F bonds combined.

6. Comparison with experiments

The dissociation fragments for PPVE and both n-$C_4F_7H_3O$ and i-$C_4F_7H_3O$ molecules were identified experimentally using the mass spectrometry in Ref. 42. The authors classified the fragments into three main categories: (1) atomic F, (2) small fluorocarbons with only one carbon and, finally, (3) large fluorocarbons containing at least two carbons. The smaller fluorocarbons were said to be the dominant fragment for PPVE, and after our simulations at 5000 K, the smaller fluorocarbon fragments outnumber the larger fluorocarbon fragments 524 to 315. The most common fragment found throughout the simulations of PPVE was CF_2, which is formed after the dissociation of the C═C bond. The other highly dissociative bond is C#3-O which creates a C_3F_7 and a C_2F_3O fragment. Both of these are found often, being the third and ninth most common fragments, respectively, but are found much less often than CF_2 due to their high likelihood to dissociate more, leading to even smaller fragments, leading to the larger number of small fragments found in the experiment.

IV. SUMMARY AND CONCLUSIONS

We investigated the dissociation dynamics of four fluorinated organic molecules in their lowest excited triplet state following electron impact excitation. The dissociation pattern of the triplet states produced by electron impact has several features that distinguish it from the dissociation for singlet states. Dissociation is very fast as the triplet states are more repulsive than the singlet states. It appears that electrophores, i.e., small parts of molecules that localize the initial triplet excitation, exist, such as the carbon—carbon double bond or the oxygen atom. The bonds containing the electrophore dissociate readily, and the proximity to the electrophore also affects the dissociation yield of other chemical bonds. Considering all molecules that have been studied by our group, we now present a preliminary list of rules for triplet state dissociation:

- The position of an oxygen atom is very important due to the hypothesized localization of triplet excitation.
- The C—O—C bonds in ethers prefer to break such that oxygen is bonded to the largest carbon chain (the presence of a double C═C bond can alter this).
- The functional group of the oxygen atom is also important, e.g., an alcohol can be used to limit C—O breaking.
- Hydrogen atoms have fairly consistent behavior in terms of being ejected very quickly. Hydrogen atoms can be used as a pseudo-buffer between the electrophore and a part of the molecule that discourages further dissociation.
- Double carbon–carbon bonds dissociate more rapidly than single carbon–carbon bonds, at least initially, and can supersede that of single C—C bonds if the C═C bond is placed next to another electrophore, such as an oxygen atom.

29 May 2025 13:06:07

© Author(s) 2025

- The effect of proximity to multiple electrophores, e.g., a C═C bond and an oxygen atom is cumulative.

Except for the alcohol $C_4H_2F_7OH$, the C–O bonds in the C—O—C electrophore are one of, if not, the most common broken bonds in a molecule. While this shows that oxygen plays a role in triplet state dissociation due to the breakage of C—O bonds, there is also a secondary effect of oxygen. We theorize that the oxygen molecule localizes the triplet state not only causing bonds containing oxygen to break but also weakening the adjacent bonds, causing them to break more often than bonds of the same type elsewhere in the molecule. This can be seen in how the different C—C and C—F bonds break for the different molecules.

Theoretically, multiple bonds and atoms could potentially play the role of an electrophore. Previously, our group showed that the double C═C bond plays the role of an electrophore, due to the small energy gap between the π bonding orbital and the π^* antibonding orbital. Any other aspect of a molecule that contains a similar energy gap, such as the lone pairs of an oxygen atom should be an electrophore, though further investigation will be needed to identify additional instances of electrophores.

In this paper, we focus on the mechanisms of dissociation and only present the data on bond breaking but not on the reaction products, channels, and branching ratios. However, the number of trajectories which lead to a particular channel and, therefore, branching ratios can be calculated from the available data similarly to how it has been done in our first paper on the topic.[4] It is also important to note again that the temperature at which these simulations are performed are significantly higher than that used experimentally and industrially. Therefore, the rules put forth in this article should be taken as preliminary rules for electron impact driven neutral dissociation via the triplet state at very high energies. Future work will involve efficient sampling techniques[55] that are required for accurate simulations at lower temperatures, down to 1000 K. The rules established in this article will then be used as a foundation and adapted to be applicable to industry relevant temperatures.

Our observations and rules suggested above can be used to aid the design of molecules with fragmentation patterns yielding the desired chemical composition of plasma for use in plasma technologies. We are currently working on improving the efficiency of our simulations, developing a faster GPU-based code and an analytical force field to replace expensive DFT on-the-fly direct dynamics, potentially utilizing machine learning, which has applications in photochemistry.[56–59] With these two improvements, we hope that the type of simulations performed by our group could become a useful tool in further understanding the mechanisms and rules of triplet state neutral dissociation in plasmas, potentially aiding fast *in silico* design of new molecules for future plasma technologies.

SUPPLEMENTARY MATERIAL

See the supplementary material for graphs comparing the dissociation yield of each bond type for each molecule considered in this paper. The number of repetitions deemed necessary for the convergence of PPVE is also compared.

ACKNOWLEDGMENTS

This work was undertaken on ARC3 and ARC4, part of the High Performance Computing facilities at the University of Leeds, UK. D. V. Shalashilin and D. V. Makhov acknowledge EPSRC support under Grant Nos. EP/P021123/1 and EP/X026973/1. D. V. Shalashilin and O. Bramley acknowledge the EPSRC IAA Grant No. EP/X52573X/1. R. Brook acknowledges the Henry Ellison, Charles Brotherton Research Scholarship. We also thank Bruce Turnbull for useful discussions.

AUTHOR DECLARATIONS

Conflict of Interest

The authors have no conflict to declare.

Author Contributions

Ryan Brook: Data curation (lead); Investigation (lead); Software (lead); Validation (lead); Visualization (equal); Writing – original draft (equal); Writing – review & editing (equal). **Oliver Bramley:** Data curation (supporting); Investigation (supporting); Visualization (supporting); Writing – original draft (equal); Writing – review & editing (equal). **Dmitry V. Makhov:** Methodology (lead); Software (supporting); Writing – original draft (equal); Writing – review & editing (equal). **Anna Nelson:** Writing – original draft (equal); Writing – review & editing (equal). **Gregory Armstrong:** Writing – original draft (equal); Writing – review & editing (equal). **Joseph Yong:** Investigation (supporting). **Ezri Saunders:** Investigation (supporting). **Johnny de Viggiani:** Investigation (supporting). **Jonathan Tennyson:** Writing – original draft (equal); Writing – review & editing (equal). **Dmitrii V. Shalashilin:** Conceptualization (lead); Funding acquisition (lead); Methodology (equal); Project administration (equal); Supervision (lead); Writing – original draft (equal); Writing – review & editing (equal).

DATA AVAILABILITY

The code used to generate the data found in this article can be found in github at https://github.com/RBrook318/PlasmaDissociation-python, Ref. 60. See also https://doi.org/10.5281/zenodo.15322947.

REFERENCES

[1]B. F. Curchod and T. Martínez, Chem. Rev. **118**, 3305 (2018).
[2]D. A. McQuarrie and J. D. Simon, *Physical Chemistry: A Molecular Approach* (University Science Books, Sausilito, 1998).
[3]F. B. Dunning and R. Hulet, *Experimental Methods in the Physical Sciences* (Academic, San Diego, 1996), Vol. 29B.
[4]D. V. Makhov, G. Armstrong, H. Chuang, H. Ambalampitiya, K. Lemishko, S. Mohr, A. Nelson, J. Tennyson, and D. Shalashilin, J. Phys. Chem. Lett. **15**, 3404 (2024).
[5]M. Barbatti *et al.*, J. Chem. Theory Comput. **18**, 6851 (2022).
[6]D. V. Makhov, K. Saita, T. J. Martinez, and D. V. Shalashilin, Phys. Chem. Chem. Phys. **17**, 3316 (2015).
[7]R. Crespo-Otero and M. Barbatti, Chem. Rev. **118**, 7026 (2018).
[8]D. V. Makhov, C. Symonds, S. Fernandez-Alberti, and D. V. Shalashilin, Chem. Phys. **493**, 200 (2017).
[9]M. Ben-Nun, J. Quenneville, and T. J. Martínez, J. Phys. Chem. A **104**, 5161 (2000).

29 May 2025 13:06:07

© Author(s) 2025

[10]B. Curchod and A. Orr-Ewing, J. Phys. Chem. A **128**, 6613 (2024).
[11]D. Metzler, R. L. Bruce, S. Engelmann, E. A. Joseph, and G. S. Oehrlein, J. Vac. Sci. Technol. A **32**, 020603 (2014).
[12]R. d'Agostino, F. Cramarossa, and F. Illuzzi, J. Appl. Phys. **61**, 2754 (1987).
[13]R. d'Agostino, F. Cramarossa, V. Colaprico, and R. d'Ettole, J. Appl. Phys. **54**, 1284 (1983).
[14]C. J. Mogab, A. C. Adams, and D. L. Flamm, J. Appl. Phys. **49**, 3796 (1978).
[15]G. S. Oehrlein *et al.*, J. Vac. Sci. Technol. B **42**, 041501 (2024).
[16]D. B. Graves *et al.*, J. Vac. Sci. Technol. B **42**, 042202 (2024).
[17]V. Donnelly and A. Kornblit, J. Vac. Sci. Technol. A **31**, 050825 (2013).
[18]L. Kline, "Dissociation processes in plasma chemistry and gaseous dielectrics," in *Gaseous Dielectrics VI* (Springer, Boston, 1991).
[19]M. Mocella, MRS Proc. **447**, 29 (1997).
[20]M. Radoiu, Radiat. Phys. Chem. **69**, 113 (2004).
[21]J. T. Houghton, Y. H. Ding, D. J. Griggs, M. Noguer, P. van der Linden, X. Dai, M. Maskell, and C. A. Johnson, *Climate Change 2001: The Scientific Basis* (Cambridge University, Cambridge, 2001).
[22]S. Pinnock, M. D. Hurley, K. P. Shine, T. J. Wallington, and T. J. Smyth, J. Geophys. Res. Atmos. **100**, 23227, https://do.org/10.1029/95JD02323 (1995).
[23]A. R. Ravishankara, S. Solomon, A. A. Turnipseed, and R. F. Warren, Science **259**, 194 (1993).
[24]H. Omori, A. Kikuchi, A. Yao, and I. Mori, *IEEE 16th International Conference on Nanotechnology (IEEE-NANO)*, Sendai, Japan, 22–25 August 2016 (IEEE, Piscataway, 2016), p. 127.
[25]T. Ichikawa, T. Takase, and N. Tamaoki, "Modeling of deposition during C5F8CO/O2/Ar plasma etching using topography and composition simulation," in *SISPAD 2007: Simulation of Semiconductor Processes and Devices* (Springer Vienna, Vienna, Austria, 2007), Vol. 123.
[26]C. Wang, B. Cooper, and J. Tennyson, Phys. Scr. **98**, 065401 (2023).
[27]H. J. Lee *et al.*, Appl. Surf. Sci. **639**, 158190 (2023).
[28]M. Cuddy and E. Fisher, ACS Appl. Mater. Interfaces **4**, 1733 (2012).
[29]K. Takahashi, A. Itoh, T. Nakamura, and K. Tachibana, Thin Solid Films **374**, 303 (2000).
[30]S. Kang, I. Sawada, Y. Kondo, and P. L. G. Ventzek, Jpn. J. Appl. Phys. **47**, 6843 (2008).
[31]V. Graves, B. Cooper, and J. Tennyson, J. Phys. B: At. Mol. Opt. Phys. **54**, 235203 (2021).
[32]K. Goswami, M. Luthra, A. K. Arora, A. Bharadvaja, and K. L. Baluja, Eur. Phys. J. D **76**, 94 (2022).
[33]K. Goswami, A. Kumar Arora, A. Bharadvaja, and K. L. Baluja, Eur. Phys. J. D **75**, 228 (2021).
[34]M. Ziółkowski, A. Vikár, M. L. Mayes, Á. Bencsura, G. Lendvay, and G. C. Schatz, J. Chem. Phys. **137**, 22A510 (2012).
[35]Y. Kumar and M. Kumar, Chem. Phys. Lett. **740**, 137071 (2020).
[36]T. Nakamura, H. Motomura, and K. Tachibana, Jpn. J. Appl. Phys. **40**, 847 (2001).
[37]B. Cooper *et al.*, Atoms **7**, 97 (2019).
[38]Z. Mašín, J. Benda, J. D. Gorfinkiel, A. G. Harvey, and J. Tennyson, Comput. Phys. Commun. **249**, 107092 (2020).
[39]S. Samukawa and T. Mukai, J. Vac. Sci. Technol. A **17**, 2463 (1999).
[40]J. Park, B. Oh, K. Kim, D. Sung, and G. Yeom, Appl. Surf. Sci. **532**, 147358 (2020).
[41]J.-H. Kim, J.-S. Park, and C.-K. Kim, ECS J. Solid State Sci. Technol. **7**, Q218 (2018).
[42]B. Mishra, M. Lily, A. K. Chandra, and R. C. Deka, J. Phys. Org. Chem. **27**, 811 (2014).
[43]T. Cha, Y. Kim, S. Lee, Y. Cho, and H. Chae, J. Vac. Sci. Technol. A **37**, 051302 (2019).
[44]T. Cha, Y. Kim, S. Lee, Y. Cho, and H. Chae, ACS Sust. Chem. Eng. **10**, 10537 (2022).
[45]S. You, E. J. Sun, Y. Hwang, and C. K. Kim, Korean. J. Chem. Eng. **41**, 1307 (2024).
[46]J. Kim, J. Park, and C. Kim, Appl. Surf. Sci. **508**, 144787 (2020).
[47]Y. Díaz-de-Mera, A. Aranda, I. Bravo, D. Rodríguez, A. Rodríguez, and E. Moreno, Environ. Sci. Pollut. Res. **15**, 584 (2008).
[48]Y. Kim, H. Kang, C. Kim, and H. Chae, ACS Sust. Chem. Eng. **11**, 6136 (2023).
[49]V. M. Freixas *et al.*, J. Chem. Theory Comput. **19**, 5356 (2023).
[50]H. Song, V. M. Freixas, S. Fernandez-Alberti, A. J. White, Y. Zhang, S. Mukamel, N. Govind, and S. Tretiak, J. Chem. Theory Comput. **17**, 3629 (2021).
[51]D. V. Makhov, W. J. Glover, T. J. Martinez, and D. V. Shalashilin, J. Chem. Phys. **141**, 054110 (2014).
[52]B. Curchod, W. J. Glover, and T. J. Martínez, J. Phys. Chem. A **124**, 6133 (2020).
[53]D. Casanova and A. Krylov, Phys. Chem. Chem. Phys. **22**, 4326 (2020).
[54]E. Epifanovsky *et al.*, J. Chem. Phys. **155**, 084801 (2021).
[55]J. Booth, S. Vazquez, E. Martinez-Nunez, A. Marks, J. Rodgers, D. R. Glowacki, and D. V. Shalashilin, Philos. Trans. R. Soc. A **372**, 20130384 (2014).
[56]J. Li and S. Lopez, Chem. Phys. Rev. **4**, 031309 (2023).
[57]S. Lin, D. Peng, W. Yang, F. L. Gu, and Z. Lan, J. Chem. Phys. **155**, 214105 (2021).
[58]J. Li, R. Stein, D. M. Adrion, and S. A. Lopez, J. Am. Chem. Soc. **143**, 20166 (2021).
[59]V. Botu and R. Ramprasad, Int. J. Quantum. Chem. **115**, 1074 (2015).
[60]R. Brook and O. Bramley (2025). "PlasmaDissociationNAMD--Python (v1.0.0)," Zenodo.

29 May 2025 13:06:07

© Author(s) 2025